



Origin of Low Ozone above Western North America: An Investigation of Sources and Trends

Ju-Mee Ryoo^{1,2}, Laura T. Iraci¹, Yu Yan Cui³, Owen R. Cooper⁴, Matthew S. Johnson¹, Kai-Lan Chang^{4,5}, Emma L. Yates^{1,2}, Valerie Thouret⁶, Hanna Clark⁶, Philippe Nedelec⁶, Bastien Sauvage⁶

¹Earth Science Division, NASA Ames Research Center, Moffett Field, CA, USA

²Bay Area Environmental Research Institute, Moffett Field, CA, USA

³The Pennsylvania State University, State College, PA; now at Environmental Defense Fund, New York, NY, USA

10 ⁴NOAA Chemical Sciences Laboratory, Boulder, CO, USA

⁵Cooperative Institute for Research in Environmental Sciences (CIRES), University of Colorado, Boulder, CO, USA

⁶Laboratoire d'Aérodynamique (LAERO), Université Toulouse, CNRS, Université de Toulouse III Paul Sabatier, 31400 Toulouse, France

Correspondence to: Ju-Mee Ryoo (ju-mee.ryoo@nasa.gov)

15 **Abstract.** While free-tropospheric ozone (O_3) over western North America (WNA) has increased since the mid-1990s, research has primarily focused on the mean. We investigate the lower tail ($O_3 < 33^{\text{rd}}$ percentile) to characterize the evolving remote background state. Because these air masses are minimally affected by episodic extremes, they offer a clearer window into long-term shifts in background O_3 , transport, and photochemistry. Using FLEXPART-ERA5 source–receptor relationships (SRRs) from 1994 to 2021, we analyze the transport history of air masses reaching WNA (25–55°N, 130–
20 90°W). Despite no robust SRR trends within the lower and mid-troposphere (0–8 km), changing emission patterns suggest an intensifying remote influence. Specifically, WNA's surface NO_x emissions have decreased while lower-tail O_3 continues to rise, aligning with increasing surface emissions from Southeast Asia and intensified shipping. In contrast, UTLS (8–13 km) SRRs show a clear increase, indicating growing influence from high-altitude sources, including enhanced transport from Southeast Asia and the tropical Pacific, and rising global aircraft emissions. GMI chemical simulations corroborate these
25 findings, revealing that net O_3 production over Southeast Asia increased by 157% in the lower troposphere and 7% in the free troposphere between 2007 and 2019. The rise in WNA's low O_3 percentiles is driven by the combined influence of intensified transport from Southeast Asia and the tropical Pacific, along with increasing global aircraft and shipping emissions. Ultimately, these trends reflect both the rapid growth of Southeast Asia emissions and shifting trans-Pacific transport.

30 1 Introduction

Tropospheric ozone (O_3) is an important trace gas because it has harmful impacts on human health and vegetation (Brauer et al., 2016; Fleming et al., 2018; Malashock et al., 2022; Mills et al., 2018). It is also an important greenhouse gas (Lacis et al., 1981; Ramaswamy, 2001; Gulev et al., 2021; IPCC, 2021) categorized as a short-lived climate forcer (Szopa et al., 2021).



Thus, it is essential to monitor tropospheric O₃ trends, analyze O₃ sources and sinks, and understand the associated
35 atmospheric transport patterns and pathways.

The first phase of the Tropospheric Ozone Assessment Report (TOAR) and the sixth Intergovernmental Panel on Climate
Change (IPCC) Assessment Report concluded that surface O₃ has increased by 30 to 70% in the mid- and high latitudes of
the Northern Hemisphere (NH) from the mid-20th century to the present day (Tarasick et al., 2019; Gulev et al., 2021). This
finding aligns with ensembles of global atmospheric chemistry models that show increasing tropospheric O₃ at northern mid-
40 latitudes, primarily driven by fossil fuel combustion and emissions of O₃ precursor gases (e.g., nitrogen oxides (NO_x = nitric
oxide [NO] + nitrogen dioxide [NO₂]), volatile organic compounds [VOCs], carbon monoxide [CO], methane [CH₄]) (Szopa
et al., 2021; Gulev et al., 2021; Fiore et al., 2022).

Since the mid-1990s O₃ has increased in the free troposphere of the NH tropics and mid-latitudes (Verstraeten et al., 2015;
Cooper et al., 2020; Gaudel et al., 2020; Gulev et al., 2021; Wang et al., 2022; Chang et al., 2022, 2023, 2024; Elshorbany et
45 al., 2024; Froidevaux et al., 2025; van Malderen et al., 2025), although trends at the surface are highly variable (Cooper et al.,
2020; Chang et al., 2023, 2025; Putero et al., 2023). In particular, positive free-tropospheric O₃ trends have been noted at the
low end of the O₃ distribution, for example at the 1st, 5th or 33rd percentiles, which have been observed in the tropics and the
mid-latitudes of the NH (Cooper et al., 2010; Cohen et al., 2018; Gaudel et al., 2020; Chang et al., 2023).

Understanding the lower tail end of the O₃ distribution is critical as it is an important component of background O₃ values.
50 Furthermore, because low-O₃ air masses are minimally affected by episodic processes—such as stratospheric intrusions and
localized urban plumes—they provide a clearer view into long-term changes in background O₃, transport, and
photochemistry. This perspective is particularly important given the observed increase at the ‘clean’ end of the O₃
distribution. Analyzing IAGOS data from 1995 to 2013, Cohen et al. (2018) found that positive trends in the northern mid-
latitude upper troposphere are driven by a significant rise in the lowest percentiles, a shift consistent with previous findings
55 (Cooper et al., 2010; Lin et al., 2015). Very low O₃ mixing ratios observed in the mid- and upper-troposphere of the mid-
latitudes also originate in the lower troposphere of remote tropical regions, where O₃ production is relatively low (Davies et
al., 1998, Grant et al., 2000; Asman et al., 2003; Cooper et al., 2010; Chang et al., 2020; Gaudel et al., 2020). A range of
atmospheric chemistry model simulations indicates that O₃ production has increased in the lower troposphere of the western
North Pacific Ocean, a region that was once dominated by O₃ destruction (Zhang et al., 2016; Lin et al., 2017; Gaudel et al.,
60 2020; Liu et al., 2022; Wang et al., 2022).

As tropospheric O₃ is an important greenhouse gas and air pollutant, understanding the changes of O₃ production in remote
regions of the world, especially in regions where O₃ destruction once dominated, improves our understanding of the global
tropospheric O₃ budget. This area of research also improves our understanding of the baseline O₃ levels that are advected
into populated regions (Ryoo et al., 2017; Jaffe et al., 2018; Columbi et al., 2023), which impact surface O₃ concentrations
65 (Lin et al., 2017) and contribute to health impacts related to O₃ exposure at high and moderate concentrations (U.S. EPA,
2020; WHO, 2021).

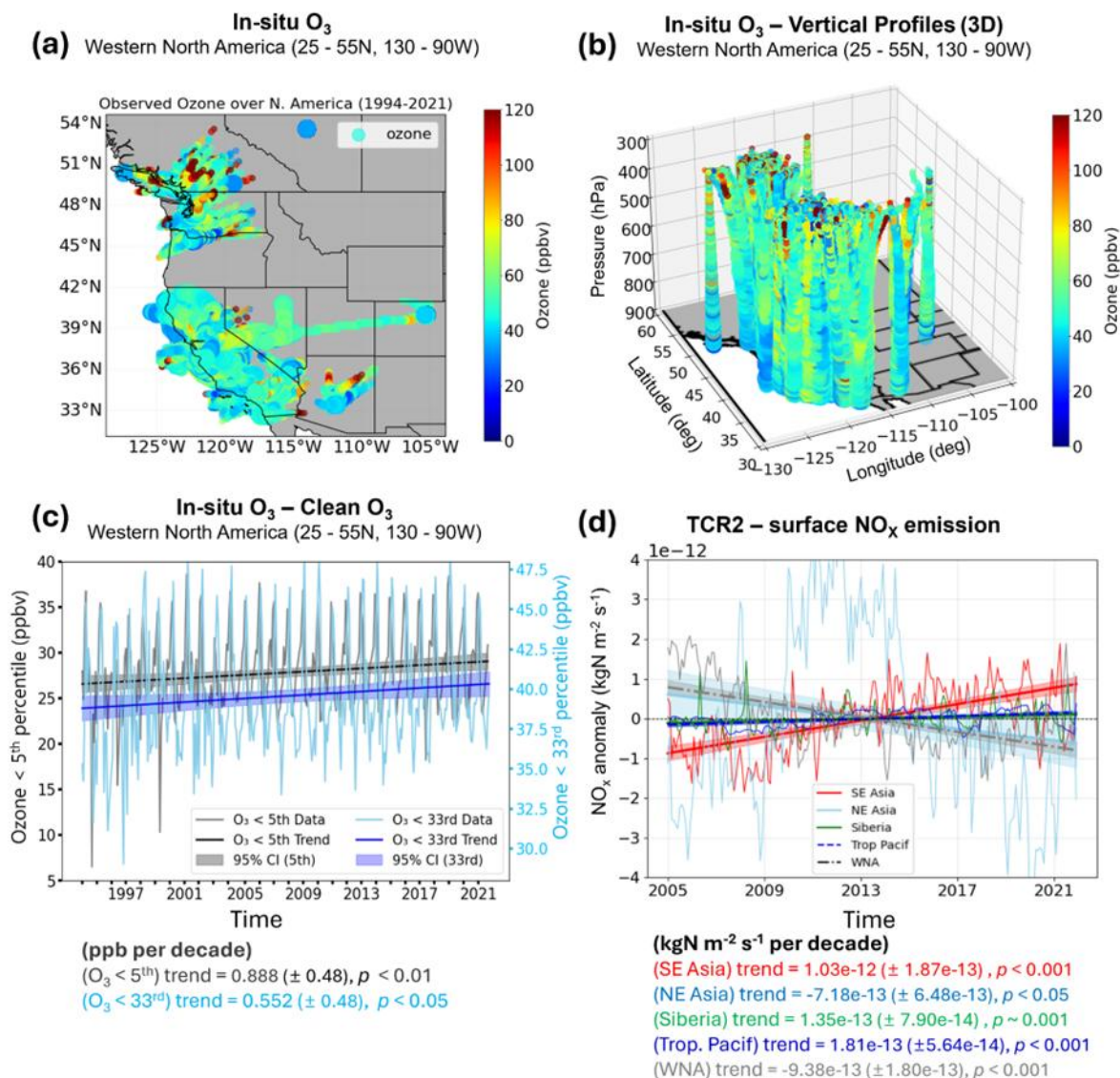


This analysis provides an update on tropospheric O₃ trends above Western North America (WNA) and explores the recent changes of O₃ production above Asia and the western North Pacific Ocean on the lower tail O₃ values advected into WNA. The primary goal of this paper is to identify the origin of the air parcels containing the lower magnitudes of O₃ above WNA, to understand how the lowest O₃ values have changed over time, and to identify whether the observed trends are driven by transport, precursor emissions, or chemical processes. We aim to answer the following three science questions:

1. *Where does the low O₃ above WNA come from?*
2. *Have the transport pathways affecting O₃ over WNA changed?*
3. *Have changes in O₃ occurred due to chemical production?*

We utilized a Lagrangian particle dispersion model to investigate trends (1994-2021; 28-year) in transport pathways of the air parcels influencing low O₃ levels above WNA and employed the Global Model Initiative (GMI) dataset (Rotman et al., 2001; Ziemke et al 2019) and Tropospheric Chemistry Reanalysis version 2 (TCR-2) chemical reanalysis (Miyazaki et al., 2019a; Miyazaki et al., 2020) to analyze changes in net chemical O₃ production in upwind source regions. For trend analysis of O₃ precursor emissions, we also used the bottom-up Community Emissions Data System (CEDS, Hoesly et al., 2018; McDuffie et al., 2020) inventory for aircraft and anthropogenic emission datasets.

The paper is structured as follows: Section 2 outlines the data and methodology employed in the study. Section 3 presents the results, and Section 4 discusses the implications of the results and their broader significance.



85

Figure. 1. Trends and uncertainty in observed O₃ and chemical reanalysis NO_x emissions: (a, b) Map of 2-D horizontal and 3-D vertical distribution of observed O₃ (circle, ppbv) over WNA used in this study (1994-2021). (c) Time series and trend (ppbv/decade) of the low O₃ (< 5th percentile (gray) and < 33rd percentile (light blue)) from 1994 to 2021. (d) Time series of monthly anomalies and trends (ppbv decade⁻¹) with uncertainty (±2 standard errors) in TCR-2 NO_x emissions over SE Asia (solid red), NE Asia (solid cyan), Siberia (solid green), the tropical Pacific (dashed blue), and WNA (gray dash-dotted) from 2005 to 2021. Shading in panels (c) and (d) denotes the 95% confidence intervals of the trends.

90



2 Data and Methodology

95 This study examines WNA (25–55°N, 130–90°W) from 1994 to 2021 (28 years). Detailed data and methodology are presented below.

2.1 FLEXPART- ERA5 (1994-2021) model output

We utilize the FLEXible PARTicle dispersion model (FLEXPART) version 10.4 particle dispersion model (Pisso et al., 2019), using meteorology from the European Centre for Medium-Range Weather Forecasts (ECMWF) Reanalysis v5
100 (ERA5). ERA5 is a fifth-generation ECMWF atmospheric meteorological reanalysis of the global atmosphere at hourly temporal resolution (Hersbach et al., 2020). Hourly and monthly data were available on a 0.25° longitude × 0.25° latitude grid with 137 vertical levels ranging from 1000 hPa to 1 hPa. We utilized 3-D wind (u, v, w), temperature, pressure, and other surface quantities (Cui et al., 2025).

FLEXPART–ERA5 generated the source-receptor relationship (SRR) quantity used in this study, which can be applied to
105 represent the air mass residence time at specific times and grid locations. Thus, this is often referred to as the '*surface influence factor*', '*residence time*', or '*retroplume*' (e.g., Cooper et al., 2010). In this study, we refer to the SRR as residence time. A high SRR indicates a strong connection between the upwind source region and the observation location. These high SRR values indicate long residence time over source regions, resulting in greater surface emission influence, while a low SRR represents a weak connection between source regions and observations due to short residence times. The model is used
110 to support our 28-year O₃ analysis from 1994 to 2021, providing a set of outputs at hourly resolution extending from the observational O₃ receptors back 15 days, with 1° × 1° spatial resolution globally (Cui et al., 2025). To track the vertical range of the SRR of trajectories associated with the O₃ observation over WNA, we classify the trajectory layers into five vertical levels: 0–300 m, 300 m–3 km, 3–8 km, 8–13 km, and 13–20 km. These five levels refer to the retroplume assessment levels associated with observed O₃ values over WNA, regardless of the original O₃ measurement altitude. While the raw data
115 contain detailed receptor and retroplume information (Cui et al., 2025), only retroplume data are retained when processing daily and monthly data.

The five vertical layers from the surface to 20 km are designed to support the investigation of the different sources associated with different altitudes and to understand their source contributions. To differentiate between source contributions, we utilize specific vertical layers: the 0–300 m and 0.3–3 km ranges quantify the respective contributions of surface-level and planetary
120 boundary layer (PBL) emissions. The 3–13 km column accounts for the influence of lightning-induced ozone formation, while the 8–13 km range isolates the impact of aircraft emissions on downwind WNA O₃ levels. The output unit of the SRR from the FLEXPART–ERA5 backward model simulation is s m³ kg⁻¹, which represents the SRR weighted by the air mass volume. For more detailed model processing information, please see Cui et al. (2025).

Daily output with 15-day back-trajectories is aggregated into monthly data by normalizing the total SRR by the O₃ receptor
125 observations. Although our initial daily output spans the globe, we restrict our monthly analysis to the NH to reduce



computational demands. We justify this by assuming that interhemispheric transport contributes relatively little to O₃ levels over WNA. To represent different atmospheric layers, the 0–300 m and 300 m – 3 km ranges were categorized as the lower troposphere, the 3–8 km range as the free troposphere, the 8–13 km range as the upper troposphere and lower stratosphere (UTLS), and the 13–20 km range as the stratosphere in the tropics and mid-latitude region.

130

2.2 Observational receptors and source regions selection

We used a data fusion technique to combine multi-platform O₃ observations across 900–300 hPa above WNA (25–55°N, 130–90°W, Figs. 1a–c), to establish our receptor list over WNA (Chang et al., 2023; Cui et al., 2025). Tropospheric O₃ observations over WNA during 1994–2021 used in this study include 1) *Ozonesonde measurements* provided by the

135

Canadian Ozonesonde Network (Environment and Climate Change Canada, 2022), and from the NOAA Global Monitoring Laboratory (NOAA GML, 2022), 2) *Lidar measurements* from Table Mountain (NASA JPL 2022), and 3) *Aircraft measurements from IAGOS* (In-Service Aircraft for a Global Observing System, 1994; Boulanger et al., 2022) and NASA AJAX/SNAX (Iraci et al., 2021; Yates et al., 2023). The availability of the observation periods varies slightly among the measurement sites during our study period from 1994–2021 (please refer to Fig. 1 of Cui et al. (2025) for more details).

140

These efforts aim to enhance accuracy and precision of O₃ trend estimates, building on earlier findings that sparse ozonesonde sampling—typically once per week—is insufficient for capturing accurate monthly means (Logan, 1999) or detecting reliable trends (Prinn, 1988). These findings were further evaluated and validated by using the densely sampled IAGOS dataset above Frankfurt, Germany (Chang et al., 2020; Saunio et al., 2012). More recently, Chang et al. (2024) demonstrated that trend estimates can vary significantly with sampling strategies, showing notable biases under sparse

145

conditions. Gaudel et al. (2024) likewise emphasized the difficulty of detecting O₃ trends in the tropics due to limited in-situ observations.

We focus on four major source regions affecting the levels over WNA: SE Asia (0–25°N, 60–130°E), NE Asia (26–46°N, 75–127°E), Siberia (50–75°N, 70–160°E), and Tropical Pacific Ocean (hereafter Tropical Pacific; 5–35°N, 180°E–130°W) because, 1) these regions reflect differing emission distributions linked to growing industries and emission control strategies

150

(Zhang et al., 2008; Wang et al., 2019), 2) these regions are well known for significantly contributing to O₃ precursor sources and sinks (Thorp et al., 2021), and 3) hemispheric-scale O₃ production and loss and its transport (Cooper et al., 2010), and biomass burning emissions transport acting as O₃ precursor species often affect WNA through long-range transport (Johnson et al., 2021) from various vertical ranges (Ryoo et al., 2017). In this analysis, we also selected the Tropical Pacific as a potential source region due to high SRR and close proximity to WNA. For examining anthropogenic shipping emissions, we

155

categorize the domain into three oceanic regions—Tropical Indian (0–30°N, 60–150°E), Tropical Pacific (5–35°N, 180°E–130°W), and mid-latitude western Pacific (30–55°N, 127–152°E). More details are shown in Section 3.3.



2.3 Other datasets

1) *GMI O₃ chemical production and loss data*: we utilized the GMI data for O₃ (Fig. S1), NO₂ (Fig. S2), and chemical O₃ production and loss to examine net O₃ production (Rotman et al., 2001; Ziemke et al. 2019). The GMI simulations employed the Modern-Era Retrospective analysis for Research and Applications, Version 2 (MERRA-2; Gelaro et al., 2017) reanalysis meteorology and a combined stratospheric-tropospheric chemical mechanism. GMI simulations have been widely used in various tropospheric studies to interpret observations of O₃ and NO_x, analyze observed trends (Ziemke et al., 2019), and investigate processes influencing O₃ (Kerr et al., 2019, 2020; Strode et al., 2015, 2016). We focused on the period from 1994 to 2019. The spatial resolution is 0.625° longitude by 0.5° latitude and monthly temporal resolution.

2) *TCR-2 NO_x emission data*: the Tropospheric Chemistry Reanalysis version 2 (TCR-2) chemical reanalysis (Miyazaki et al., 2019a; Miyazaki et al., 2020) constrained by satellite chemical observations provides a broad range of chemical components, including surface concentrations of various species including O₃ and NO_x and anthropogenic and natural (e.g., lightning, biomass burning) emissions (Lahoz and Schneider, 2014). TCR-2 data have been evaluated against independent observations (e.g., Miyazaki et al., 2019b; Thompson et al., 2019). We utilize NO_x emission data across multiple sectors—including surface anthropogenic, lightning, and biomass burning sources (Figs. 1d, S2)—to demonstrate that the rising O₃ over WNA is likely driven by remote transport rather than local emissions. Specifically, while surface NO_x over WNA has trended downward, the lower tail of the O₃ distribution shows an increase (Figs. 1c, d), suggesting a disconnect between local precursor trends and the evolving remote background. The spatial resolution of the data is 1.125° longitude x 1.125° latitude, with monthly data available from 2005 to 2021.

3) *CEDS anthropogenic and aircraft NO_x emissions*: the Community Earth atmospheric Data System (CEDS) emissions inventory was used to estimate anthropogenic and aircraft NO_x emissions over the source regions (Smith et al., 2015). The system focuses on emissions of aerosol (BC, OC), gases (SO₂, NH₃) and O₃ precursor compounds (NO_x, CH₄, CO, VOC). The inventory resolution is monthly, 0.5°×0.5° spatial resolution, and 25 altitude levels, ranging from 0.305 to 14.495 km above sea level (Hoesly et al., 2018; McDuffie et al., 2020).

Data from the GMI model and TCR-2 chemical reanalysis were applied to assess trends in O₃ (Fig. S1 in the supplementary material) and its precursor species such as NO_x (Fig. 1d, Fig. S2).

2.4 Analysis Methodology

The number of receptors varies across years due to sampling differences in observational data availability. To account for this variability, we normalized the monthly SRRs by dividing the total SRRs from the receptors by the total receptor count for each month across different altitudes. Monthly O₃ concentration percentiles from 1994 to 2021 were then defined relative to the monthly percentiles determined during the 2004–2014 baseline period. This period was selected as a representative baseline for O₃ values at receptors over WNA because O₃ sampling during this time was relatively evenly distributed.



We categorized O₃ values based on the following percentiles: O₃ < 5th percentile, 5th ≤ O₃ < 33rd percentile, 33rd ≤ O₃ < 50th percentile, 50th ≤ O₃ < 66th percentile, 66th ≤ O₃ < 95th percentile, and O₃ ≥ 95th percentile. We defined low O₃ using the 33rd percentile threshold, as SRR patterns were largely similar to those below the 5th percentile. To avoid the air masses with the strongest impact from stratospheric intrusion, we also excluded the 95-100th percentiles in our analysis.

The total number of monthly non-zero SRRs across the full range of O₃ values from 1994 to 2021 was N = 539,808 out of 553,608 total gridded O₃ observation (Cui et al., 2025). Of this total, the number of SRRs associated with O₃ values below the 5th percentile and the 33rd percentile is N = 26,858 and 173,538, respectively, while those above the 66th percentile total N = 187,597, across all vertical layers. Those for high O₃ (66th–95th percentile), excluding the highest O₃ levels that are typically associated with recent stratospheric intrusions, is N = 160,299.

To analyze trends in air mass transport associated with particular O₃ levels above WNA, as represented by SRR, we applied a linear regression model. For each month, the monthly SRR values corresponding to the O₃ percentile ranges, as described in Section 2.1, were input into the linear regression model, formulated as follows:

$$SRR_{(x,y,z)} = M(x, y, z) + \tau(x, y, z) \times t + \varepsilon \quad (1)$$

where x is longitude, y is latitude, z is the five vertical layers, $M(x, y, z)$ is a monthly mean cycle, $\tau(x, y, z)$ is the trend coefficient, which is shown in the results, t represents the total 336 months (12 months x 28 years), and ε represents the residual term. The p -value of the trend estimate was used to assess the trend reliably. We adopted the TOAR statistical guidelines where a trend with p -value ≤ 0.05 is considered to be high certainty (Chang et al., 2023b; Wasserstein et al., 2019). Monthly average SRRs (M) were first calculated for the five vertical layers at each longitude and latitude grid point from 1994 to 2021. Trends were then determined using a deseasonalized dataset, by subtracting the 28-year mean for each month ($M(x, y, z)$) from the corresponding monthly SRR (e.g., for January 2010, the anomaly was calculated by subtracting the average of each January from 1994 to 2021 from the January 2010 value). Similarly, the trend of net GMI O₃ production is also computed following Eq. (1). Net O₃ production was estimated by subtracting all O₃ loss terms from all O₃ production terms, based on the GMI dataset.

The percentage change in chemical net O₃ production (ΔO_{3_netp}) is calculated in Eq. (2) based on the difference in the averages of the two periods (P1: 1994–2006 and P2: 2007–2019) normalized by their combined average during the P1 period:

$$\Delta O_{3_netp} = \frac{O_{3_netp(P2:2007-2019)} - O_{3_netp(P1:1994-2006)}}{abs(O_{3_netp(P1:1994-2006)})} \times 100(\%) \quad (2)$$

$O_{3_netp(1994-2006)}$ represents the average net O₃ production for P1, and $O_{3_netp(2007-2019)}$ represents the average net O₃ production for P2 for the specified four source regions over the free and lower troposphere, respectively.

To quantify the spatial influence of different source regions on low O₃ levels over WNA, we calculated the normalized mean density (we call this as “relative intensity”). This value represents the mean SRR of air masses with positive net O₃ production for a specific region, normalized against the hemispheric average (0–90°N)—SE Asia, NE Asia, Siberia, and the



220 Tropical Pacific—during two time periods: P1 (1994–2006) and P2 (2007–2021). These values were derived from two-dimensional joint probability density functions (2D joint PDFs), estimated using a non-parametric, gaussian kernel density estimation (KDE) method, to estimate the PDF of a variable (Chen et al., 2017), implemented via the SciPy library in Python v3.7. Specifically, the relative intensity of *region i* during a given time was computed as $(\text{KDE}(\text{region } i, \text{time}) / \text{KDE}(\text{total, time})) \times 100 (\%)$, where $\text{region } i \in \{\text{SE Asia, NE Asia, Siberia, Tropical Pacific}\}$.

225 Results were also tested across multiple bandwidths (i.e., smoothing parameters for KDE). The optimal bandwidth values were determined using the leave-one-out cross-validation (LOOCV) method, also implemented via the SciPy library. This approach minimizes the estimated error of the KDE by iteratively computing the density estimator on all but one data point and then evaluating its ability to obtain the density of the left-out point, ultimately selecting the bandwidth that minimizes the total error across all data points. Uncertainty in the computed relative intensity for each sector was also assessed using

230 bootstrap-estimated standard deviation ($N=1000$).

3 Results

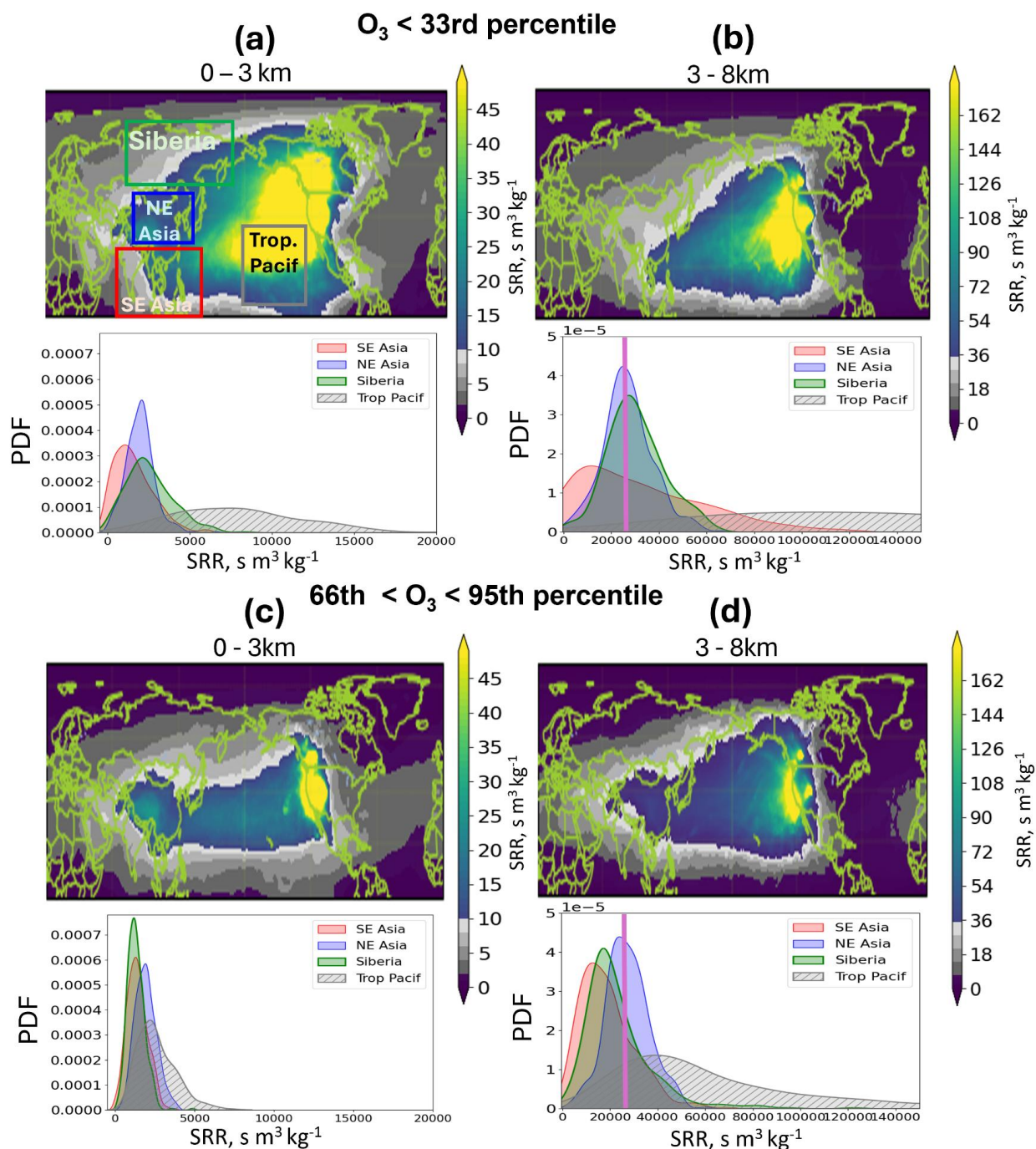
3.1 Where does the low O₃ come from?

Figure 2 illustrates the SRR maps and corresponding latitudinal probability density functions (PDFs) for low (<33rd percentile) and high (66th-95th percentile) O₃ concentrations across the lower (0–3 km) and middle (3–8 km) troposphere. By

235 integrating the spatial maps with the PDF distributions, we identify distinct transport corridors associated with varying O₃ levels. In the lower troposphere (0–3 km), low O₃ air masses exhibit high SRR values, with PDF peaks and dispersions aligned specifically with the southern regions of East Asia and the tropical Pacific (Fig. 2a; SRR is higher in the red and gray boxed regions on the map and in the corresponding red and gray shaded areas of the PDFs than in Fig. 2c). Conversely, elevated O₃ concentrations are primarily associated with air masses transiting through NE Asia (Fig. 2c).

240 This latitudinal contrast is further amplified in the free troposphere (3–8 km). While SRR values are generally larger in this layer compared to the lower troposphere, the spatial patterns remain consistent (Figs. 2b, d). For lower O₃ percentiles, air parcels predominantly traverse the tropical eastern Pacific and SE Asia. In contrast, higher O₃ percentiles are linked to air masses with extended SRR in the midlatitudes (15–45°N), exhibiting transport pathways that originate or pass through NE Asia. Notably, air masses associated with these higher O₃ levels show an increasing trend in midlatitude SRR over the study

245 period across all vertical layers (Fig. S3). These characteristic transport dynamics are also evident on a seasonal basis (Fig. S4), confirming that the geographic origin of the air mass is an important factor of O₃ variability over WNA.



250 **Figure 2.** Maps of the source-receptor relationship (SRR) and their distributions: (a) FLEXPART-ERA5 SRR and Probability density function (PDF) of SRR over SE Asia (red), NE Asia (blue), Siberia (green) and Tropical Pacific (gray) for (top) low O_3 ($< 33^{\text{rd}}$ percentile), (bottom) high O_3 ($66^{\text{th}} - 95^{\text{th}}$ percentile) over the WNA for (a, c) 0–3 km



level and (b, d) 3–8 km. The red, blue, green, and gray boxes in (a) represent SE Asia (0–25°N, 60–130°E), NE Asia (26–46°N, 75–127°E), Siberia (50–75°N, 70–160°E), and Tropical Pacific (5–35°N, 180°E–130°W), respectively. The vertical magenta line represents the $SRR > 25000 \text{ s m}^3 \text{ kg}^{-1}$.

255

3.2 Have transport pathways changed?

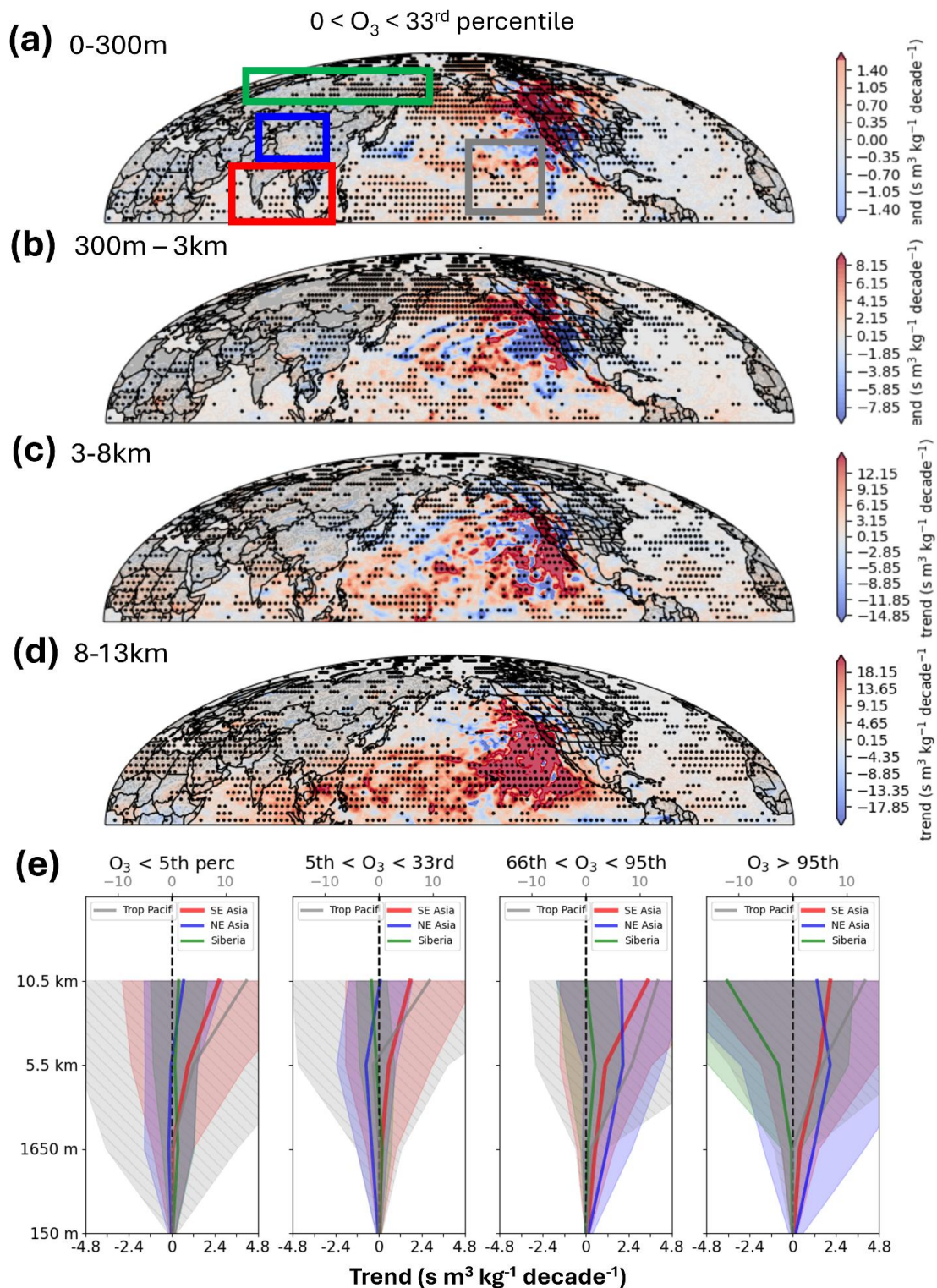
To examine transport trends on decadal scales, we analyze the SRR patterns for air parcels containing low free tropospheric O_3 amounts over WNA. Figure 3 illustrates trends in the SRR of low- O_3 air parcels from the lower and the free troposphere to the UTLS. For low O_3 , SRRs show no clear trend in the lower troposphere (Figs. 3a-b) or in the free troposphere (Fig. 3c) in the regions of interest. In contrast, low O_3 SRR exhibits an increasing tendency across all regions in the UTLS, though with large variability (Figs. 3d, e).

260

SRR for high O_3 (66th–95th percentile, Fig. 3e) observations over WNA exhibit more positive trends and large variability. For example, SRR from NE Asia for high O_3 , both in the lower troposphere and the free troposphere, shows a distinct increasing trend (Figs. 2(c, d), Fig. 3e, Fig. S3). Conversely, high- O_3 SRR shows a decreasing trend at higher latitudes (e.g., Siberia), while over the Tropical Pacific it exhibits increasing trend with substantial variability (Fig. 3e).

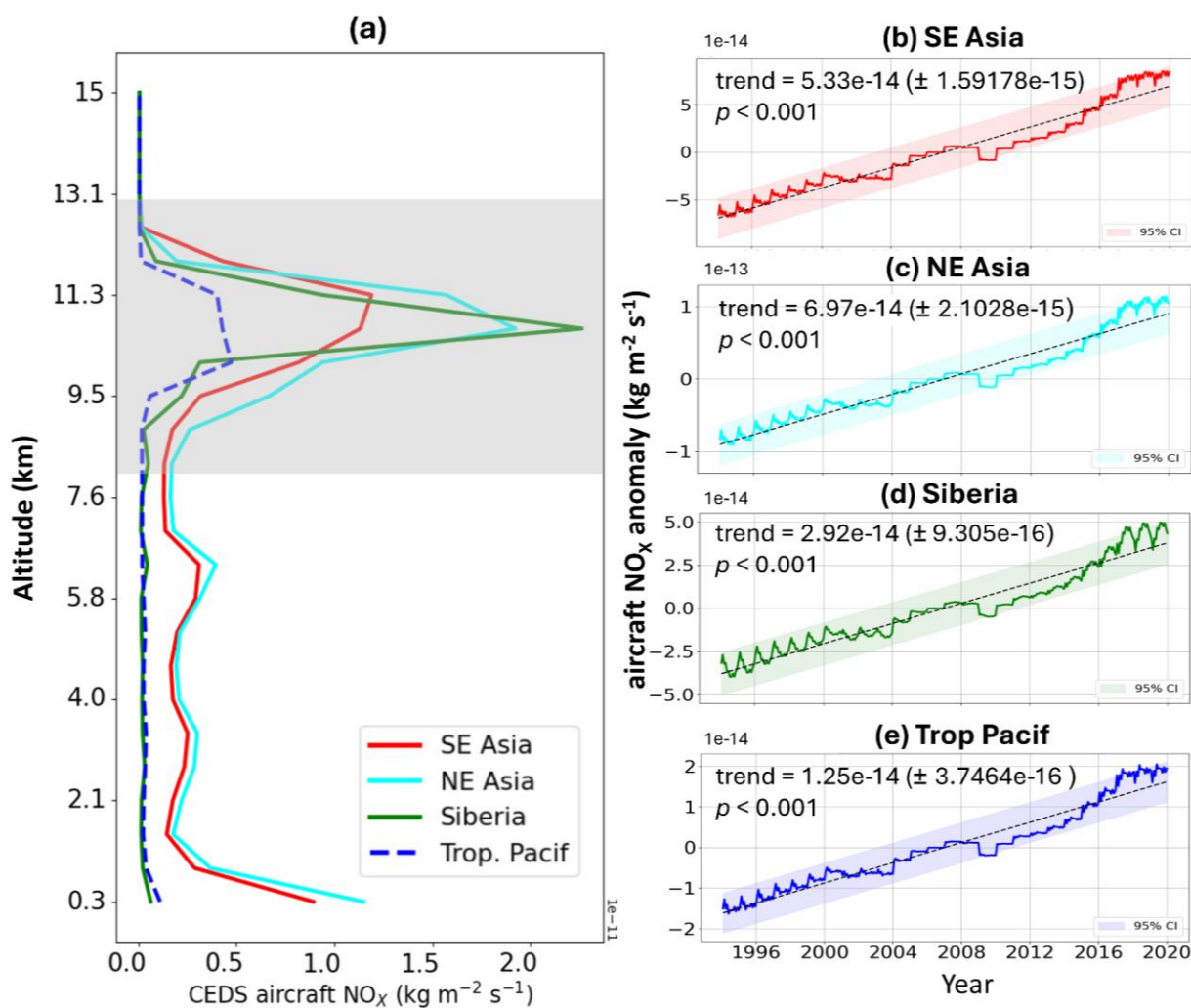
265

An increasing trend in the UTLS SRR of air masses is evident in Fig. 3 (8–13 km, Fig. 3d and 3e), influencing both low and high O_3 over WNA.





270 **Figure 3. Trends in SRR over the interval 1994 – 2021. Panels (a) - (d) show SRR trends for low O₃ (5th to 33rd**
percentile range) over WNA for air parcels originating from four different layers: (a) 0–300 m, (b) 300 m–3 km, (c)
3–8 km, and (d) 8–13 km. Red colors identify regions of increasing influence. The dots on the maps represent the grid
cells with a *p-value* < 0.05. The red, blue, green, and gray boxes in (a) represent SE Asia, NE Asia, Siberia, and
Tropical Pacific, respectively. Panel (e) shows the vertical distribution of SRR trends for four regions (SE Asia, NE
275 Asia, Siberia, and Tropical Pacific) and four categories of ozone amount: O₃ < 5th percentile, 5th < O₃ < 33rd
percentiles, 66th < O₃ < 95th, and O₃ > 95th percentile. The trend values for the tropical Pacific are shown on the upper
x-axis (gray), while those for the other regions are shown on the lower x-axis (black). The shaded region in (e)
represents the ±2 standard deviation (2σ) of each trend value at the given level for the region. For ease of
visualization, the mid-level height of each layer is shown on the y-axis in panel (e).



280

Figure 4. (a) Vertical profiles of CEDS aircraft NO_x emission (kg m⁻² s⁻¹) averaged over 1994-2019. (b-e) Time series of monthly anomaly and their linear trends (lines, kg m⁻² s⁻¹ per decade) with uncertainty (± 2 standard errors) of the CEDS aircraft NO_x emissions in the UTLS (~8–13 km) over the four source regions during 1994-2019. Shading in (b-e) denotes 95% confidence intervals.

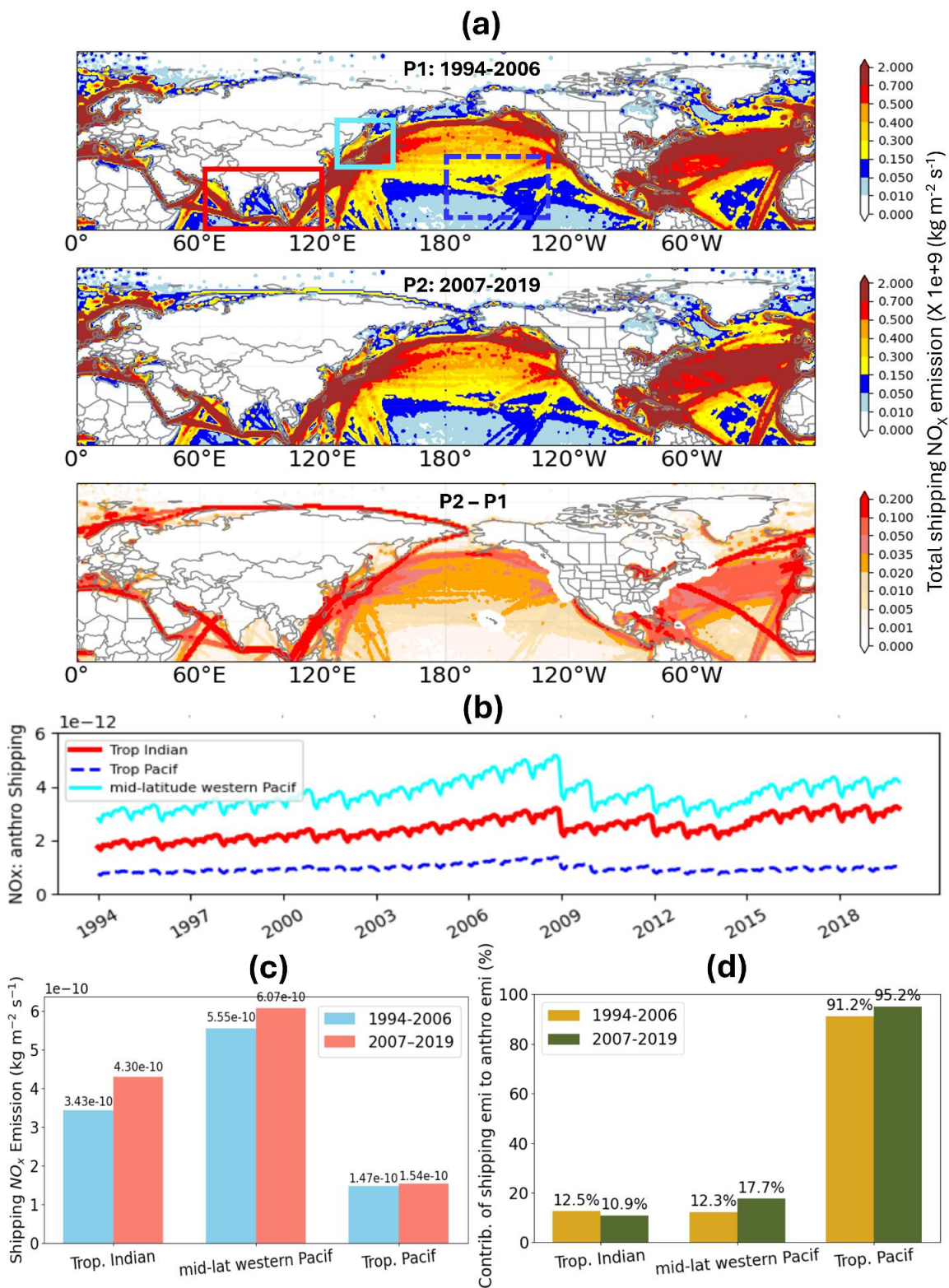
285

3.3 Are changes in O₃ due to changes in emissions or chemical production?

To further investigate the potential cause of increasing amounts of O₃ in the lowest percentiles at 8-13 km, we examine aircraft emissions averaged over 1994-2019, as shown in Fig. 4a. Notably, aircraft emissions—which have increased steadily across source regions (Fig. 4b)—typically peak within the 8–13 km range, coinciding with the primary cruising altitudes of



290 commercial aviation. This finding aligns with Eastham et al. (2024), who demonstrated that the impact of civil aviation is
driven primarily by a hemispheric-scale tropospheric O₃ response to NO_x rather than by localized effects.
Beyond aviation emissions, we also find from GMI simulations that lightning-NO_x shows increasing patterns over SE Asia
and North America within the free troposphere and UTLS (3–13 km) (see Fig. 5 of Cui et al., 2025). These results further
support the findings of Gressent et al. (2014), who identified additional sources—such as lightning-generated nitrogen
295 oxides—as important contributors to O₃ variability.



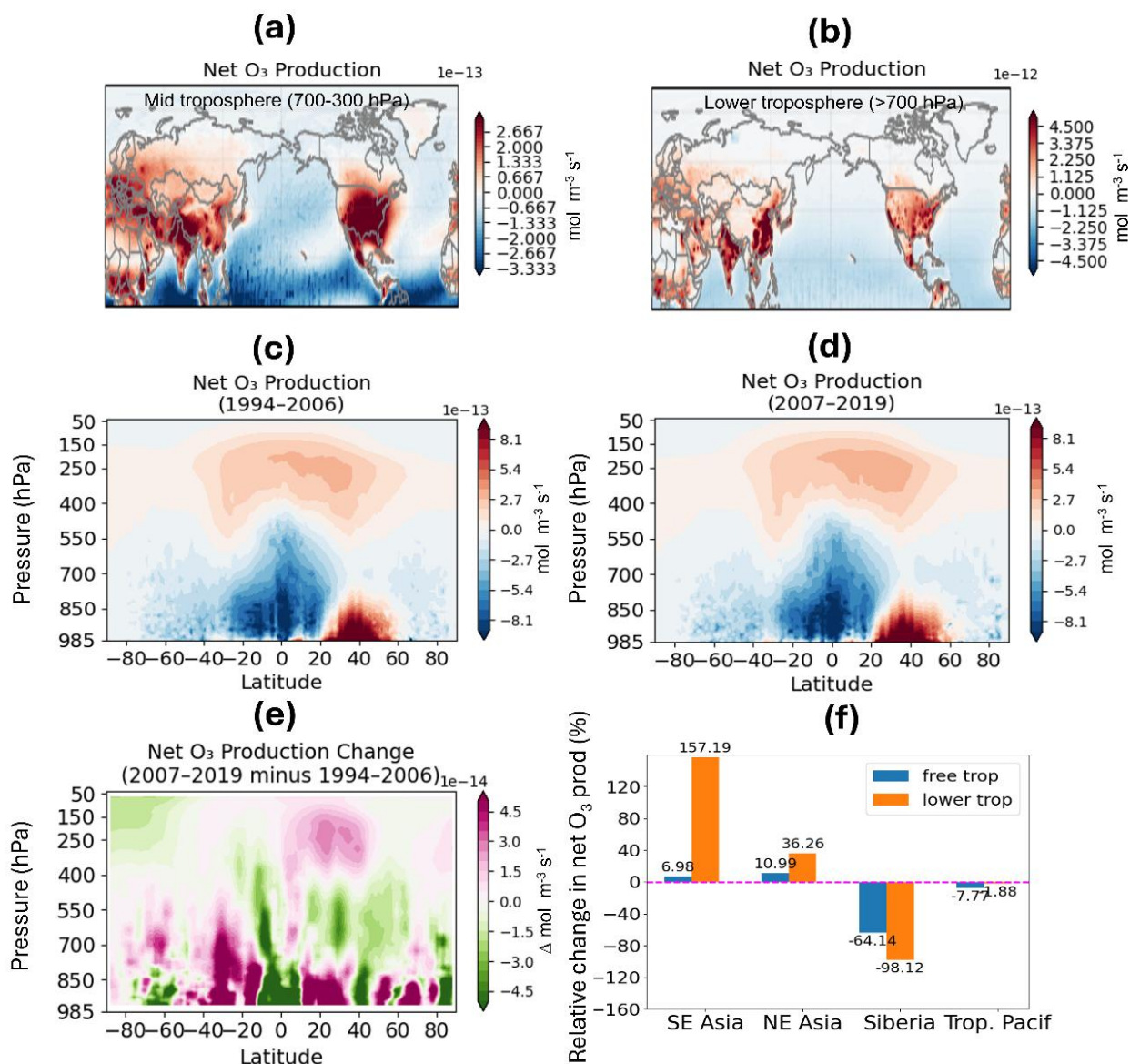


300 **Figure 5. (a) Maps of CEDS anthropogenic shipping NO_x emissions (kg m⁻² s⁻¹) for (top) P1 (1994–2006), (middle) P2 (2007–2019), and (bottom) the difference (P2 – P1). (b) Time series of shipping NO_x emissions for three source regions: the tropical Indian Ocean (0–30°N, 60–150°E; solid red), tropical Pacific (5–35°N, 180–130°W; dashed blue), and midlatitude western Pacific (30–55°N, 127–152°E; solid cyan). (c) Mean shipping emissions (kg m⁻² s⁻¹) and (d) the contribution of shipping emissions to total anthropogenic emissions (%) over the three source regions during P1 and P2. The tropical Indian, tropical Pacific, and midlatitude western Pacific regions are indicated in red, blue, and cyan, respectively.**

305

While Fig. 3 shows an upward trend in transport from the tropical Pacific UTLS, the rise in low O₃ over WNA is not solely driven by aircraft emissions. In fact, aircraft emissions are quite low in this specific area (Fig. 4a). This observation instead suggests the influence of other emission sources. To investigate additional anthropogenic emissions over our source regions, we particularly examined shipping emissions. As shown in Fig. 5, shipping emissions are high over the Tropical Indian Ocean (including the SE Asia region) and the Tropical Pacific. While the decrease in global shipping NO_x emissions around 310 2009 was likely not driven by a single factor, the observed NO_x reduction in 2009 has been reported to be partially associated with the 2008 global economic recession (Tong et al., 2016; Fig. 5b).

During the recent period (P2), total shipping emissions show a slight increase over the tropical Indian Ocean and the midlatitude western Pacific (including Northeast Asia), with minor changes over the tropical Pacific. Relative to total 315 anthropogenic emissions, shipping contributes up to 10.9%, 17.7%, and 95.2% in these regions, respectively, highlighting the growing role of shipping emissions there. (Fig. 5d).



320 **Figure 6. (a) Map of GMI net chemical O₃ production (mol m⁻³ s⁻¹) in the (a) free-troposphere (700 - 288.88 hPa) and (b) lower troposphere (725-985 hPa) during 1994-2019. (c-e) Zonal-mean latitude–height cross sections of net O₃ production during (c) the early period (P1: 1994-2006) and (d) the later period (P2: 2007-2019). (e) the difference from (d) to (c); contours are smoothed by averaging within a 5° latitude × 50 hPa grid cell. (f) relative percent change in zonal-mean GMI chemical net O₃ production from P1 to P2.**

325 Given that both transport and chemical processes can influence O₃ levels over WNA, we further analyze trends in net O₃ chemical production to distinguish the role of chemical processes using GMI. Figure 6 represents the net O₃ chemical



production obtained by subtracting GMI O₃ loss from GMI O₃ production across the NH and the four distinct regions (Fig. S1) in both the free troposphere and the lower troposphere. In the lower troposphere, net O₃ production is typically an order of magnitude higher than in the free troposphere, with positive values occurring predominantly over densely populated regions of the NH, while net destruction is mainly observed over the tropical ocean (Figs. 6a, b).

To further assess temporal changes in net O₃ production in the lower and free troposphere, we calculate the change in net O₃ production between the early period (P1: 1994–2006) and the later period (P2: 2007–2019), as shown in Figs. 6(e-f). The zonal-mean latitude–height cross sections of net O₃ production during P1 and P2 reveal several key features: i) a consistent positive net O₃ production over 20–35°N in the lower troposphere during both periods (Fig. S5, S6); ii) a notable increase in net O₃ production in the extended upper tropospheric and lower stratospheric region in recent years (pink color in panel (e) centered around 20° N and around 300-150 hPa) (P2, Fig. S6), along with a decrease in net O₃ production over the tropical Pacific (green color extending up from the surface, centered on the equator). These results are broadly consistent with Archibald et al. (2020), who reported O₃ production from the UK Chemistry and Aerosol Community Climate Model (UKCA; Luhar et al., 2018) for the year 2000. However, slight differences in the magnitude and pattern of extratropical zonal-mean net O₃ production may stem from our study's longer analysis period (1994–2019) and the use of a different model. During the later period (P2), a significant increase and positive trend in ΔO_{3_netp} (net O₃ production difference) is observed, particularly at the low-tropospheric level over NE and SE Asia (Fig. S5), with the rate reaching up to ~157% over SE Asia (Fig. 6f).

O₃ net production and destruction vary significantly by region (Figs. 6a-b), influenced by a combination of natural and human-caused factors. A study led by Thorp et al. (2021), for instance, found that in western Siberia, surface O₃ is controlled by a dynamic interplay of seasonal atmospheric transport patterns, a dominant sink from dry deposition by forest vegetation, and the prevalence of anthropogenic emissions from the transport and energy sectors. However, note that this is the net O₃ production in a particular model grid cell, and does not account for transport from the stratosphere, surface deposition or transport of O₃ from one region to another.

350

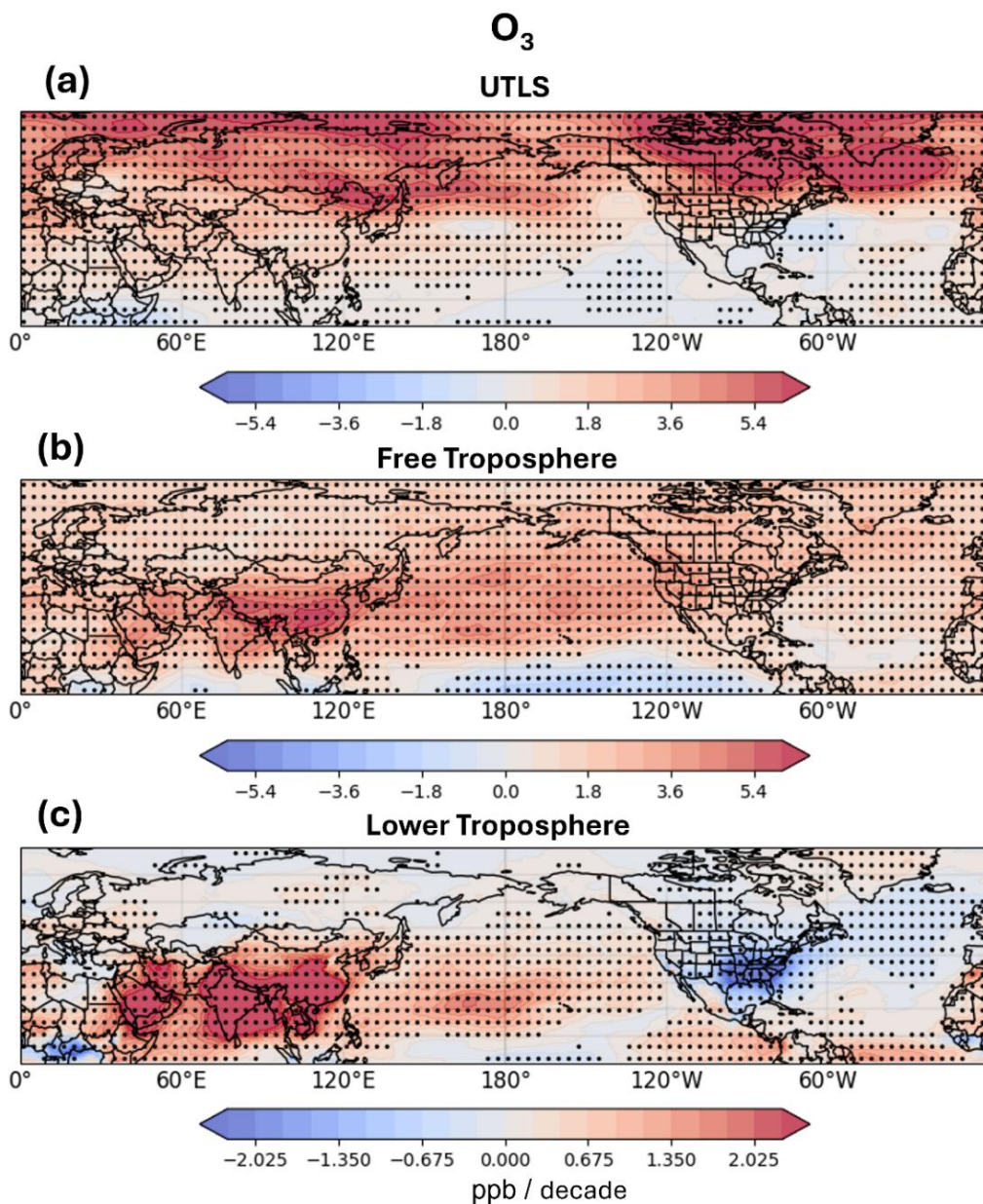


Figure 7. GMI O₃ trend (ppb decade⁻¹) in the (a) UTLS (244.88–176.93 hPa), (b) free troposphere (700–288.88 hPa), and (c) lower troposphere (725–985 hPa) calculated from 1994 and 2019. The dots on the maps represent the grid cells with a *p*-value < 0.05. The pressure shown here represents the midpoint of each GMI model level.

355

Overall, Fig. 6 suggests that chemical ΔO_3_{netp} over East Asia has shown a significant increase in recent years, particularly over SE Asia in the lower troposphere. To investigate the temporal evolution of O₃ increases in more extended vertical layers,



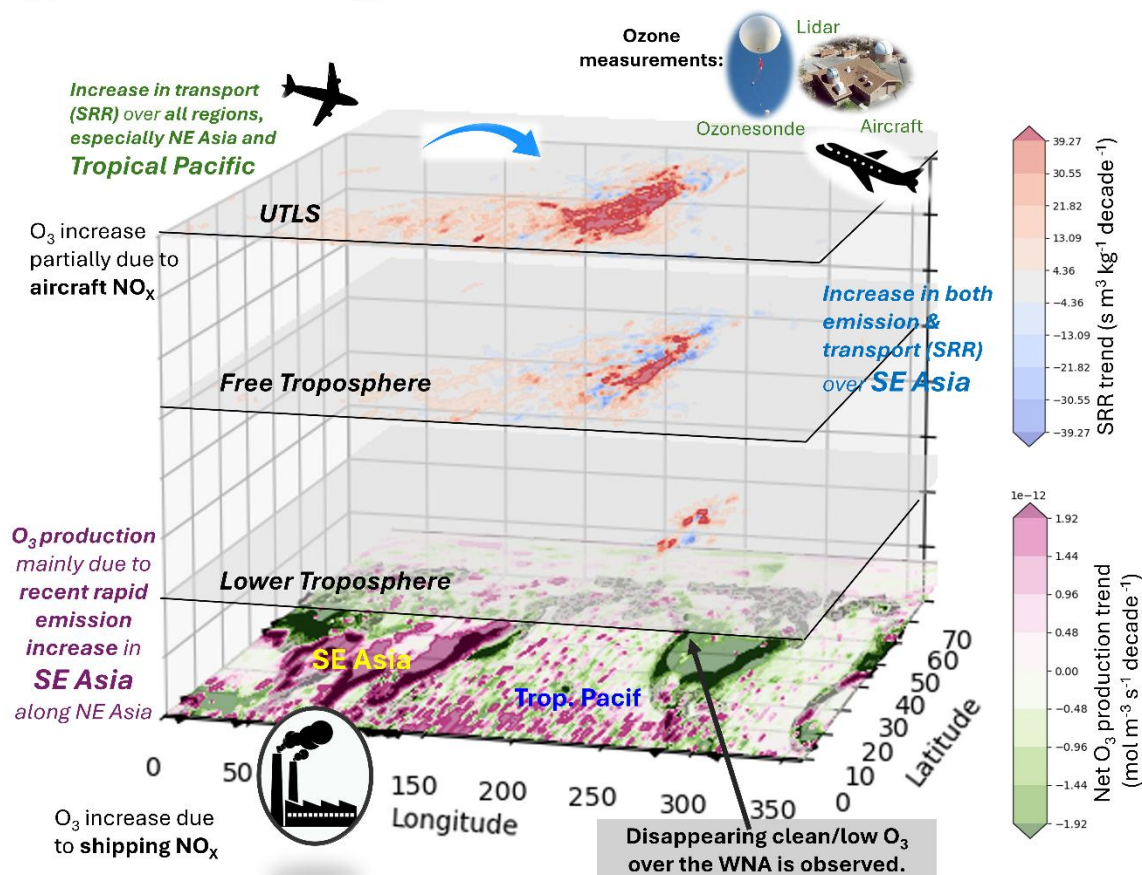
Fig. 7 illustrates the trends for O₃ across the three vertical layers. In the tropics, tropospheric O₃ exhibits an overall increasing trend, particularly over East Asia, consistent with the findings of Ziemke et al. (2019).

360 In the UTLS (Fig. 7a), O₃ growth rates tend to increase at high latitudes, partially reflecting the influence of stratospheric processes. Conversely, large variability is observed in the extratropics due to a complex interplay between dynamic processes and O₃ chemistry (Cooper et al., 2004; Bak et al., 2025). The pattern is different in the free troposphere with positive trends in O₃ across most of the NH. Strongest increases stretch from South and East Asia across the North Pacific Ocean to WNA, while decreases are limited to the equatorial region (Fig. 7b). The increase in O₃ growth rate in the free
365 troposphere and the decrease in the lower troposphere shown in Fig. 7 are overall consistent with and supported by observed O₃ trends (Chang et al., 2023; Fig. S1). In addition, O₃ shows increases over SE Asia and the Pacific Ocean but decreases over North America, aligning with IAGOS dataset trends reported by Gaudel et al. (2020). Similar patterns are also found in net O₃ production trends (Fig. S5-S7).

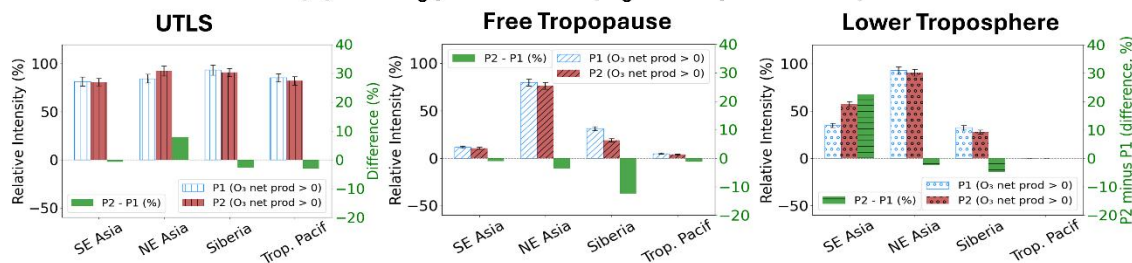
The schematics in Fig. 8 summarize our findings on the key regions contributing to low O₃ over WNA. Regional net O₃
370 production analysis indicates that SE Asia's contribution to low O₃ (< 33rd percentile) levels over WNA—driven by both SRR and chemical production—has intensified in recent years (P2: 2007–2021) compared to the earlier period (P1: 1994–2006). This increase is most pronounced in the lower troposphere, where relative O₃ production rose by approximately 23% (Fig. 8b), with the highest positive net production centered over SE and NE Asia (Fig. S6). While net O₃ production from SE Asia also increased within the free troposphere, the magnitude of change was less substantial (Fig. 8b). In contrast, the
375 UTLS exhibits positive net O₃ production across nearly all regions. This widespread increase is linked to rising aircraft emissions (Fig. 4) and enhanced SRR (Fig. 3)—a result consistent with the hemispheric-scale response described by Eastham et al. (2024). Notably, the tropical Pacific also shows entirely positive net O₃ production within this upper layer.



(a) Schematics of Low O₃ (< 33rd percentile) and its transport trend over WNA



(b) Net O₃ production (O₃ < 33rd percentile)



380

Figure 8. (a) Trends in low O₃ net production and transport (1994–2019). Decadal trends in net O₃ production (mol m⁻³ s⁻¹ decade⁻¹) and transport (SRR; s m³ kg⁻¹ decade⁻¹) specifically for the low O₃ (<33rd percentile) over western North America (WNA). (b) Normalized mean density of net O₃ production associated with low O₃ (<33rd percentile) SRR, shown relative to the NH total across the (left) UTLS, (center) free troposphere, and (right) lower troposphere.



385 **Data are grouped by early (P1: 1994–2006; blue hatched) and later (P2: 2007–2019; brown hatched) periods, with their difference (P2–P1; green). Error bars indicate $\pm 1\sigma$ via bootstrap resampling.**

4 Discussion

There have been many studies linking rising emissions and increasing O_3 in the tropics. Zhang et al. (2016) showed that increased O_3 production in the tropics is driving the increase of O_3 at mid-latitudes. This is consistent with our finding that
390 positive net O_3 production is also found across the UTLS, free-, and low tropospheric tropical region ($\sim 5^\circ N$; Fig. 6 and Fig. 8). We also found that the influence of transport (SRR) tends to increase in the UTLS region for cases of both low and high O_3 amounts (see Fig. 3).

Our analysis included the subtropical and mid-latitude regions, where atmospheric dynamics are more complex and not solely driven by convection, providing a broader, potentially dynamic impact on tropospheric O_3 (Lin et al., 2014, 2015,
395 2017; Xue et al., 2020; Oman et al., 2011; 2013, Chandra et al., 1998; Ziemke et al., 2015; Cooper et al., 2013; Jeong et al., 2023). In this context, we also investigated the potential role of El Niño Southern Oscillation (ENSO) and Quasi Biannual Oscillation (QBO) effects on SRR and their impact on low tropospheric O_3 over WNA, but with SRR only, we could not detect a significant influence (not shown). However, the role of emissions sectors, photochemical reactions during transport, climate variability, and meteorological factors (Xue et al., 2020) in both local and long-range transport warrants further
400 exploration in future studies.

While we did not conduct a detailed investigation of seasonal variability in SRR, it was evident that SRR patterns shift northward from DJF (December–January–February) to JJA (June–July–August) due to synoptic variability and changes in the jet stream position (Figs. S8, S9). For example, peak SRR and its variability align with the subtropical jet in DJF ($\sim 30^\circ N$) but shift to the mid-latitude jet in JJA ($\sim 45^\circ N$) (Fig. S9). Extended SRR and transport near the jet location are closely linked
405 to O_3 seasonality and variability. This aligns with Barnes and Fiore (2013), who found that a poleward shift in the jet stream results in a similar poleward shift in O_3 variability, with lower standard deviations in O_3 levels farther from the jet. The application of FLEXPART-ERA5 SRRs, along with our analysis method, could serve as a framework for future studies to further investigate seasonal variations in tropospheric O_3 trends over WNA.

Regarding the increase in chemical O_3 production, the increase in SE and NE Asia emissions, as shown in Fig. 6, coincides
410 with a rapid rise in methane (CH_4) concentrations (Nisbet et al., 2016, 2019). This trend may be linked to the overall increase in emissions across Asia (Kurokawa and Ohara, 2020) and a possible suppression of hydroxyl radical (OH) levels during that period. The CH_4 –OH feedback mechanism could have further contributed to rising CH_4 concentrations (Zhao et al., 2020; He et al., 2026). However, given that the response of O_3 to CH_4 increases is relatively slow and modest (Fiore et al., 2008), further investigation is also needed. The chemical pathways involved in O_3 formation are more complex and require further
415 studies.



As discussed in Fig. 6, the increased O₃ production in SE Asia is closely linked to rising anthropogenic emissions (Li et al., 2024) and can largely be attributed to shipping as well as biomass burning (Fig. S2). A recent study by Liu et al. (2024) highlights the significant roles of biomass burning and urbanization in increasing NO_x emissions over South, SE, and East Asia. Their findings, based on Ozone Monitoring Instrument (OMI) observations, indicate that biomass burning NO_x emission levels are nearly double those reported in existing model inventories. As shown in Fig. S2, however, biomass-burning NO_x from TCR-2 is relatively smaller than that from other sources, suggesting its overall impact is likely limited, although a more quantitative analysis is needed to assess its quantitative effect on O₃.

5 Summary and Conclusions

We investigated the spatial and chemical origins of air parcels with observed low O₃ over western North America (WNA; 25–55°N, 130–90°W) using the FLEXPART-ERA5 model for the period 1994–2021. We found that air masses associated with low O₃ primarily originate from the tropical Pacific and Southeast (SE) Asia. While no clear long-term trends were identified in the source–receptor relationships (SRRs) for the lower and free troposphere, SRRs increased in the upper troposphere–lower stratosphere (UTLS; ~8–13 km). This enhancement increases the potential influence of lightning (Cui et al., 2025) and aircraft emissions on low-O₃ conditions over WNA.

Consistent with recent increases in aircraft emissions, the contribution of aviation to O₃ over WNA under low-ozone conditions has strengthened. In addition, between 2007 and 2019, Global Model Initiative (GMI) simulations show a notable increase in net O₃ chemical production over SE Asia, increasing up to 157% in the lower troposphere and 7% in the free troposphere. Furthermore, increasing SRRs from FLEXPART-ERA5 associated with positive net O₃ chemical production over SE and Northeast (NE) Asia in the UTLS and free troposphere partially explain the observed increase in low O₃ over WNA.

Another key novel contribution of our study is the focus on distinct O₃ levels (based on percentiles) rather than the entire O₃ distribution, with the significant finding that in the free troposphere, ozone amounts over WNA are increasing in even the smallest O₃ percentiles - a trend closely linked to rising emissions in SE Asia. For example, during 2007–2021, the positive net O₃ production associated with low O₃ (< 33rd percentile) has increased by about 23% over SE Asia in the lower troposphere. Additionally, we found consistently positive O₃ production over the Tropical Pacific, with longer SRR affecting lesser O₃ values over WNA. This coincides with increasing shipping emissions in the lower troposphere and aircraft emissions in the UTLS of the tropical Pacific.

We also extend the springtime analysis of Cooper et al. (2010) by incorporating the whole year (Fig. S3 with providing seasonal variation) and a longer study period, demonstrating a continuing trend of Asian emission influence on O₃ levels over WNA. Our findings also highlight a distinctly different transport pattern, with enhanced transport from NE Asia contributing to high O₃ levels over WNA. Furthermore, our combined analysis of SRR and chemical processes underscores



the importance of monitoring O₃ transport in conjunction with changes in atmospheric circulation, long-range transport, and shifts in both local and remote anthropogenic emissions at regional and global scales.

450 Finally, the gridded O₃ database developed in this study—derived from a wide range of tropospheric O₃ measurements (900–300 hPa) and combined with backward Lagrangian transport model simulations using FLEXPART-ERA5 (Cui et al., 2025)—enables investigation of the source regions associated with different O₃ percentiles observed over WNA.

Data availability

The data used in this study are openly available at the following URL/DOI: ERA5 meteorological reanalysis data are
455 available from the Copernicus Climate Change Service (<https://cds.climate.copernicus.eu/datasets>). The Tropospheric Chemistry Reanalysis (TCR-2) data for 2005–2021 is freely available at <https://doi.org/10.25966/9qgv-fe81>. The MERRA-2 GMI simulation is available at <https://acd-ext.gsfc.nasa.gov/Projects/GEOSCCM/MERRA2GMI/>. CEDS Aircraft Emissions (Version 2021-04-21) gridded over a 0.5° latitude x 0.5° longitude grid, with 25 altitude levels are available on
460 <https://zenodo.org/records/7846185>. The OMI total ozone data including discussion of data quality are available from <https://ozoneaq.gsfc.nasa.gov/>. The MLS data used to obtain SCO were derived from their v4.2 ozone profiles (<https://mls.jpl.nasa.gov/eos-aura-mls/data.php>). The FLEXPART-ERA5 model outputs both daily and monthly data, associated receptor data, and post-processing scripts is available at NASA's ASDC (<https://asdc.larc.nasa.gov/project/WNA-BackTraj>).

Supplement link

465 Supplementary material is provided in a separate document.

Author contributions

LI, JR, YC, MJ, and OC conceptualized and designed the research. YC and JR carried out the experiments, with initial field data collected and processed by KC and EY. YC developed and executed the model simulations, while JR conducted the data analysis and visualization. JR prepared the manuscript with contributions and revisions from all co-authors.

470 Competing interests

The authors declare that they have no conflict of interest.



Acknowledgements

This work is supported at NASA Ames Research Center. We thank the NASA ACCDAM program for providing support and resources (20-ACCDAM20-0083). The authors would like to acknowledge the NASA High-End Computing (HEC) Program through the NASA Advanced Supercomputing (NAS) Division at Ames Research Center (award SMD-20-28429430). K.-L. Chang acknowledges additional support from NOAA cooperative agreement NA22OAR4320151. IAGOS data were created with support from the European Commission, national agencies in Germany (BMBF), France (MESR), and the UK (NERC), and the IAGOS member institutions (<http://www.iagos.org/partners>). The participating airlines (Lufthansa, Air France, Austrian, China Airlines, Hawaiian Airlines, Air Canada, Iberia, Eurowings Discover, Cathay Pacific, Air Namibia, Sabena) supported IAGOS by carrying the measurement equipment free of charge since 1994. The data are available at <http://www.iagos.fr> thanks to additional support from AERIS.

References

- Archibald, A. T., Neu, J. L., Elshorbany, Y., Cooper, O. R., Young, P. J., Akiyoshi, H., Cox, R. A., Coyle, M., Derwent, R., Deushi, M., Finco, A., Frost, G. J., Galbally, I. E., Gerosa, G., Granier, C., Griffiths, P. T., Hossaini, R., Hu, L., Jöckel, P., Josse, B., Lin, M. Y., Mertens, M., Morgenstern, O., Naja, M., Naik, V., Oltmans, S., Plummer, D. A., Revell, L. E., Saiz-Lopez, P., Saxena, P., Shin, Y. M., Shahid, I., Shallcross, D., Tilmes, S., Trickl, T., Wallington, T. J., Wang, T., Worden, H. M., and Zeng, G.: Tropospheric Ozone Assessment Report: A critical review of changes in the tropospheric ozone burden and budget from 1850 to 2100, *Elem. Sci. Anth.*, 8, 1, <https://doi.org/10.1525/elementa.2020.034>, 2020.
- Asman, W. A. H., Lawrence, M. G., Brenninkmeijer, C. A. M., Crutzen, P. J., Cuijpers, J. W. M., and Nédélec, P.: Rarity of upper-tropospheric low O₃ mixing ratio events during MOZAIC flights, *Atmos. Chem. Phys.*, 3, 1541–1549, 2003.
- Bak, J., Kim, J., Koo, H., Pan, L. L., Ryoo, M., Newman, P. A., Franchin, A., Liu, X., Abad, G. G., Lee, J., Jeon, W., and Kim, H.: An Integrated Analysis of Ozone and Carbon Monoxide Over the Western Pacific Using Satellite and Aircraft Measurements During the ACCLIP Summer Campaign 2022, *J. Geophys. Res.-Atmos.*, 130, e2024JD042771, <https://doi.org/10.1029/2024JD042771>, 2025.
- Barnes, E. A. and Fiore, A. M.: Surface ozone variability and the jet position: Implications for projecting future air quality, *Geophys. Res. Lett.*, 40, 2839–2844, <https://doi.org/10.1002/grl.50411>, 2013.
- Becker, J. S., DeLang, M. N., Chang, K.-L., Serre, M. L., Cooper, O. R., Schultz, M. G., Schröder, S., Lu, X., Zhang, L., Deushi, M., Josse, B., Keller, C. A., Lamarque, J.-F., Lin, M., Liu, J., Marécal, V., Strode, S. A., Sudo, K., Tilmes, S., Zhang, L., Brauer, M., and West, J. J.: Using Regionalized Air Quality Model Performance and Bayesian Maximum Entropy data fusion to map global surface ozone concentration, *Elem. Sci. Anth.*, 11, 1, <https://doi.org/10.1525/elementa.2022.00025>, 2023.
- Brauer, M., Freedman, G., Frostad, J., van Donkelaar, A., Martin, R. V., Dentener, F., van Dingenen, R., Estep, K., Amini, H., Apte, J. S., Balakrishnan, K., Barregard, L., Broday, D., Feigin, V., Ghosh, S., Hopke, P. K., Knibbs, L. D., Kokubo, Y.,



- Liu, Y., Ma, S., Morawska, L., Sangrador, J. L., Shaddick, G., Anderson, H. R., Vos, T., Forouzanfar, M. H., Burnett, R. T.,
505 and Cohen, A.: Ambient Air Pollution Exposure Estimation for the Global Burden of Disease 2013, *Environ. Sci. Technol.*,
50, 79–88, <https://doi.org/10.1021/acs.est.5b03709>, 2016.
- Chandra, S., Ziemke, J. R., Min, W., and Read, W. G.: Effects of 1997–1998 El Niño on tropospheric ozone and water
vapor, *Geophys. Res. Lett.*, 25, 3867–3870, 1998.
- Chang, K.-L., Cooper, O. R., Gaudel, A., Petropavlovskikh, I., and Thouret, V.: Statistical regularization for trend detection:
510 An integrated approach for detecting long-term trends from sparse tropospheric ozone profiles, *Atmos. Chem. Phys.*, 20,
9915–9938, <https://doi.org/10.5194/acp-20-9915-2020>, 2020.
- Chang, K.-L., Cooper, O. R., Gaudel, A., Allaart, G., Ancellet, G., Clark, H., Godin-Beekmann, S., Leblanc, T., Van
Malderen, R., Nédélec, P., Petropavlovskikh, I., Steinbrecht, W., Stübi, R., Tarasick, D. W., and Torres, C.: Impact of the
515 COVID-19 economic downturn on tropospheric ozone trends: an uncertainty weighted data synthesis for quantifying
regional anomalies above western North America and Europe, *AGU Advances*, 3, e2021AV000542,
<https://doi.org/10.1029/2021AV000542>, 2022.
- Chang, K.-L., Cooper, O. R., Rodriguez, G., Iraci, L. T., Yates, E. L., Johnson, M. S., and West, J. J.: Diverging ozone
trends above western North America: Boundary layer decreases versus free tropospheric increases, *J. Geophys. Res.-Atmos.*,
128, e2022JD038090, <https://doi.org/10.1029/2022JD038090>, 2023a.
- 520 Chang, K.-L., Schultz, M. G., Koren, G., and Selke, N.: Guidance note on best statistical practices for TOAR analyses, arXiv
[preprint], <https://arxiv.org/abs/2304.14236>, 2023b.
- Chang, K.-L., Cooper, O. R., Gaudel, A., Petropavlovskikh, I., Effertz, P., Morris, G., and McDonald, B. C.: Technical note:
Challenges in detecting free tropospheric ozone trends in a sparsely sampled environment, *Atmos. Chem. Phys.*, 24, 6197–
6218, <https://doi.org/10.5194/acp-24-6197-2024>, 2024.
- 525 Chang, K.-L., McDonald, B. C., Harkins, C., and Cooper, O. R.: Surface ozone trend variability across the United States and
the impact of heat waves (1990–2023), *Atmos. Chem. Phys.*, 25, 5101–5132, <https://doi.org/10.5194/acp-25-5101-2025>,
2025.
- Chen, Y.-C.: A Tutorial on Kernel Density Estimation and Recent Advances, *Biostatistics & Epidemiology*, 1, 161–187,
<https://doi.org/10.1080/24709360.2017.1396742>, 2017.
- 530 Chou, C. C.-K., Liu, S. C., Lin, C.-Y., Shiu, C.-J., and Chang, K.-H.: The trend of surface ozone in Taipei, Taiwan, and its
causes: Implications for ozone control strategies, *Atmos. Environ.*, 40, 3898–3908,
<https://doi.org/10.1016/j.atmosenv.2006.04.018>, 2006.
- Christiansen, A., Mickley, L. J., and Hu, L.: Constraining long-term NO_x emissions over the United States and Europe using
nitrate wet deposition monitoring networks, *Atmos. Chem. Phys.*, 24, 4569–4589, <https://doi.org/10.5194/acp-24-4569-2024>,
535 2024.
- Cohen, Y., Petetin, H., Thouret, V., Marécal, V., Josse, B., Clark, H., Sauvage, B., Fontaine, A., Athier, G., Blot, R.,
Boulangier, D., Cousin, J.-M., and Nédélec, P.: Climatology and long-term evolution of ozone and carbon monoxide in the



- upper troposphere–lower stratosphere (UTLS) at northern midlatitudes, as seen by IAGOS from 1995 to 2013, *Atmos. Chem. Phys.*, 18, 5415–5453, <https://doi.org/10.5194/acp-18-5415-2018>, 2018.
- 540 Colombi, N. K., Jacob, D. J., Yang, L. H., Zhai, S., Shah, V., Grange, S. K., Yantosca, R. M., Kim, S., and Liao, H.: Why is ozone in South Korea and the Seoul metropolitan area so high and increasing?, *Atmos. Chem. Phys.*, 23, 4031–4044, <https://doi.org/10.5194/acp-23-4031-2023>, 2023.
- Cooper, M. J., Martin, R. V., Livesey, N. J., Degenstein, D. A., and Walker, K. A.: Analysis of satellite remote sensing observations of low ozone events in the tropical upper troposphere and links with convection, *Geophys. Res. Lett.*, 40, 3761–
- 545 3765, <https://doi.org/10.1002/grl.50698>, 2013.
- Cooper, O. R., Forster, C., Parrish, D., Dunlea, E., Hübler, G., Fehsenfeld, F., Holloway, J., Oltmans, S., Johnson, B., Wimmers, A., and Horowitz, L.: On the life-cycle of a stratospheric intrusion and its dispersion into polluted warm conveyor belts, *J. Geophys. Res.*, 109, D23S09, <https://doi.org/10.1029/2003JD004006>, 2004.
- Cooper, O. R., Parrish, D. D., Stohl, A., Trainer, M., Nédélec, P., Thouret, V., Cammas, J. P., Oltmans, S. J., Johnson, B. J.,
- 550 Tarasick, D., Leblanc, T., McDermid, I. S., Jaffe, D., Gao, R., Stith, J., Ryerson, T., Aikin, K., Campos, T., Weinheimer, A., and Avery, M. A.: Increasing springtime ozone mixing ratios in the free troposphere over western North America, *Nature*, 463, 344–348, <https://doi.org/10.1038/nature08708>, 2010.
- Cooper, O. R., et al.: Global distribution and trends of tropospheric ozone: An observation-based review, *Elem. Sci. Anth.*, 2, 000029, <https://doi.org/10.12952/journal.elementa.000029>, 2014.
- 555 Cooper, O. R., Schultz, M. G., Schröder, S., Chang, K.-L., Gaudel, A., Carbajal Benítez, G., Cuevas, E., Fröhlich, M., Galbally, I. E., Kubistin, D., Lu, X., McClure-Begley, A., Molloy, S., Nédélec, P., O’Brien, J., Oltmans, S. J., Petropavlovskikh, I., Ries, L., Senik, I., Sjöberg, K., Solberg, S., Spain, T. G., Spangl, W., Steinbacher, M., Tarasick, D., Thouret, V., and Xu, X.: Multi-decadal surface ozone trends at globally distributed remote locations, *Elem. Sci. Anth.*, 8, 23, <https://doi.org/10.1525/elementa.420>, 2020.
- 560 Cooper, O. R., Ziemke, J. R., and Chang, K.-L.: Tropospheric Ozone [in “State of the Climate in 2023”], *Bull. Amer. Meteor. Soc.*, 105, S94–S96, <https://doi.org/10.1175/BAMS-D-24-0116.1>, 2024.
- Cui, Y. Y., Ryoo, J.-M., Johnson, M. S., Chang, K.-L., Yates, E. L., Cooper, O. R., and Iraci, L. T.: Global source–receptor-relationship database for integrated tropospheric ozone observations from multiplatform datasets in western North America during 1994–2021, *Earth Syst. Sci. Data*, 17, 5903–5914, <https://doi.org/10.5194/essd-17-5903-2025>, 2025.
- 565 Davies, W. E., Vaughan, G., and O’Connor, F. M.: Observation of near-zero ozone concentrations in the upper troposphere at mid-latitudes, *Geophys. Res. Lett.*, 25, 1173–1176, 1998.
- Elshorbany, Y., Ziemke, J. R., Strode, S., Petetin, H., Miyazaki, K., De Smedt, I., Pickering, K., Seguel, R. J., Worden, H., Emmerichs, T., Taraborrelli, D., Cazorla, M., Fadnavis, S., Buchholz, R. R., Gaubert, B., Rojas, N. Y., Nogueira, T., Salameh, T., and Huang, M.: Tropospheric ozone precursors: global and regional distributions, trends, and variability,
- 570 *Atmos. Chem. Phys.*, 24, 12225–12257, <https://doi.org/10.5194/acp-24-12225-2024>, 2024.



- Eastham, S. D., Chossière, G. P., Speth, R. L., Jacob, D. J., and Barrett, S. R. H.: Global impacts of aviation on air quality evaluated at high resolution, *Atmos. Chem. Phys.*, 24, 2687–2703, <https://doi.org/10.5194/acp-24-2687-2024>, 2024.
- Environment and Climate Change Canada: Canadian ozonesonde network [Dataset], World Ozone and Ultraviolet Radiation Data Centre (WOUDC), <https://hegiftom.meteo.be/datasets/ozonesondes>, 2022.
- 575 Fiore, A. M., West, J. J., Horowitz, L. W., Naik, V., and Schwarzkopf, M. D.: Characterizing the tropospheric ozone response to methane emission controls and the benefits to climate and air quality, *J. Geophys. Res.*, 113, D08307, <https://doi.org/10.1029/2007JD009162>, 2008.
- Fiore, A. M., et al.: Global air quality and climate, *Chem. Soc. Rev.*, 41, 6667–6685, <https://doi.org/10.1039/c2cs35095f>, 2012.
- 580 Fiore, A. M., Hancock, S. E., Lamarque, J.-F., Correa, G. P., Chang, K.-L., Ru, M., Cooper, O. R., Gaudel, A., Polvani, L. M., Sauvage, B., and Ziemke, J. R.: Understanding recent tropospheric ozone trends in the context of large internal variability: A new perspective from chemistry-climate model ensembles, *Environ. Res. Climate*, 1, 025008, <https://doi.org/10.1088/2752-5295/ac9cc2>, 2022.
- Fleming, Z. L., et al.: Tropospheric Ozone Assessment Report: Present-day ozone distribution and trends relevant to human health, *Elem. Sci. Anth.*, 6, 12, <https://doi.org/10.1525/elementa.273>, 2018.
- 585 Froidevaux, L., et al.: Tropical upper-troposphere trends in ozone and carbon monoxide (2005-2020): observational and model results, *Atmos. Chem. Phys.*, 25, 597–621, <https://doi.org/10.5194/acp-25-597-2025>, 2025.
- Fry, M. M., et al.: The influence of ozone precursor emissions from four world regions on tropospheric composition and radiative climate forcing, *J. Geophys. Res.*, 117, D07306, <https://doi.org/10.1029/2011JD017134>, 2012.
- 590 Gaudel, A., et al.: Aircraft observations since the 1990s reveal increases of tropospheric ozone at multiple locations across the Northern Hemisphere, *Sci. Adv.*, 6, eaba8272, <https://doi.org/10.1126/sciadv.aba8272>, 2020.
- Gaudel, A., Bourgeois, I., Li, M., Chang, K.-L., Ziemke, J., Sauvage, B., Stauffer, R. M., Thompson, A. M., Kollonige, D. E., Smith, N., Hubert, D., Keppens, A., Cuesta, J., Heue, K.-P., Veeffkind, P., Aikin, K., Peischl, J., Thompson, C. R., Ryerson, T. B., Frost, G. J., McDonald, B. C., and Cooper, O. R.: Tropical tropospheric ozone distribution and trends from in situ and satellite data, *Atmos. Chem. Phys.*, 24, 9975–10000, <https://doi.org/10.5194/acp-24-9975-2024>, 2024.
- 595 Gelaro, R., et al.: The Modern-Era Retrospective Analysis for Research and Applications, Version 2 (MERRA-2), *J. Climate*, 30, 5419–5454, <https://doi.org/10.1175/JCLI-D-16-0758.1>, 2017.
- Grant, W. B., Browell, E. V., Butler, C. F., Fenn, M. A., Clayton, M. B., Hannan, J. R., Fuelberg, H. E., Blake, D. R., Blake, N. J., Gregory, G. L., Heikes, B. G., Sachse, G. W., Singh, H. B., Snow, J., and Talbot, R. W.: A case study of transport of tropical marine boundary layer and lower tropospheric air masses to the northern midlatitude upper troposphere, *J. Geophys. Res.*, 105, 3757–3769, 2000.
- 600 Gressent, A., Sauvage, B., Defer, E., Pätz, H. W., Thomas, K., Holle, R., Cammas, J.-P., Nédélec, P., Boulanger, D., Thouret, V., and Volz-Thomas, A.: Lightning NO_x influence on large-scale NO_y and O₃ plumes observed over the northern mid-latitudes, *Tellus B*, 66, 25544, <https://doi.org/10.3402/tellusb.v66.25544>, 2014.



- 605 Gulev, S. K., et al.: Changing State of the Climate System, in: *Climate Change 2021: The Physical Science Basis. Contribution of Working Group I to the Sixth Assessment Report of the Intergovernmental Panel on Climate Change*, edited by: Masson-Delmotte, V., et al., Cambridge University Press, Cambridge, UK and New York, NY, USA, 287–422, <https://doi.org/10.1017/9781009157896.004>, 2021.
- Hall, K. R., Wang, H., Souri, A. H., Liu, X., and Chance, K.: Ozone anomalies in dry intrusions associated with atmospheric
610 rivers, *J. Geophys. Res.-Atmos.*, 129, e2023JD039949, <https://doi.org/10.1029/2023JD039949>, 2024.
- He, J., Naik, V., and Horowitz, L. W.: Interpreting changes in global methane budget in a chemistry-climate model constrained with methane and isotopic observations. *AGU Advances*, 7, e2025AV001822. <https://doi.org/10.1029/2025AV001822>, 2026.
- Hersbach, H., et al.: The ERA5 global reanalysis, *Q. J. Roy. Meteor. Soc.*, 146, 1999–2049, <https://doi.org/10.1002/qj.3803>,
615 2020.
- Hoesly, R. M., Smith, S. J., Feng, L., Klimont, Z., Janssens-Maenhout, G., Pitkanen, T., Seibert, J. J., Vu, L., Andres, R. J., Bolt, R. M., Bond, T. C., Dawidowski, L., Kholod, N., Kurokawa, J.-I., Li, M., Liu, L., Lu, Z., Moura, M. C. P., O'Rourke, P. R., and Zhang, Q.: Historical (1750–2014) anthropogenic emissions of reactive gases and aerosols from the Community Emissions Data System (CEDS), *Geosci. Model Dev.*, 11, 369–408, <https://doi.org/10.5194/gmd-11-369-2018>, 2018.
- 620 Holmes, C. D., Prather, M. J., Søvde, O. A., and Myhre, G.: Future methane, hydroxyl, and their uncertainties: key climate and emission parameters for future predictions, *Atmos. Chem. Phys.*, 13, 285–302, <https://doi.org/10.5194/acp-13-285-2013>, 2013.
- IPCC: *Climate Change 2021: The Physical Science Basis. Contribution of Working Group I to the Sixth Assessment Report of the Intergovernmental Panel on Climate Change*, edited by: Masson-Delmotte, V., et al., Cambridge University Press, Cambridge, United Kingdom and New York, NY, USA, 2391 pp., <https://doi.org/10.1017/9781009157896>, 2021.
- 625 Iraci, L. T., Yates, E. L., Marrero, J. E., Parworth, C. L., Ryoo, J.-M., Tanaka, T., et al.: Airborne Trace Gas Measurements Collected by the Alpha Jet Atmospheric eXperiment (AJAX) Project: 2011–2018 [Dataset], Atmospheric Science Data Center, https://doi.org/10.5067/ASDC/AJAX_O3, 2021.
- Jacob, D. J., Logan, J. A., and Murti, P. P.: Effect of rising Asian emissions on surface ozone in the United States, *Geophys. Res. Lett.*, 26, 2175–2178, <https://doi.org/10.1029/1999GL900450>, 1999.
- 630 Jaffe, D. A., Cooper, O. R., Fiore, A. M., Henderson, B. H., Tonnesen, G. S., Russell, A. G., et al.: Scientific assessment of background ozone over the U.S.: Implications for air quality management, *Elem. Sci. Anth.*, 6, 56, <https://doi.org/10.1525/elementa.309>, 2018.
- Jaffe, D. A., Ninneman, M., and Chan, H. C.: NO_x and O₃ trends at U.S. non-attainment areas for 1995–2020: Influence of
635 COVID-19 reductions and wildland fires on policy-relevant concentrations, *J. Geophys. Res.-Atmos.*, 127, e2021JD036385, <https://doi.org/10.1029/2021JD036385>, 2022.
- Jeong, Y., Kim, S.-W., Kim, J., Shin, D., Kim, J., Park, J.-H., and An, S.-I.: Influence of ENSO on tropospheric ozone variability in East Asia, *J. Geophys. Res.-Atmos.*, 128, e2023JD038604, <https://doi.org/10.1029/2023JD038604>, 2023.



- Johnson, M. S., Strawbridge, K., Knowland, K. E., Keller, C., and Travis, M.: Long-range transport of Siberian biomass
640 burning emissions to North America during FIREX-AQ, *Atmos. Environ.*, 252, 118241,
<https://doi.org/10.1016/j.atmosenv.2021.118241>, 2021.
- Kenyon, K. E.: North Pacific High: an hypothesis, *Atmos. Res.*, 51, 15–34, [https://doi.org/10.1016/S0169-8095\(98\)00110-0](https://doi.org/10.1016/S0169-8095(98)00110-0),
1999.
- Kerr, G. H., Waugh, D. W., and Miller, S. M.: Jet stream-surface tracer relationships: Mechanism and sensitivity to source
645 region, *Geophys. Res. Lett.*, 48, e2020GL090714, <https://doi.org/10.1029/2020GL090714>, 2021.
- Knowland, K. E., Ott, L. E., Duncan, B. N., and Wargan, K.: Stratospheric intrusion-influenced ozone air quality
exceedances investigated in the NASA MERRA-2 Reanalysis, *Geophys. Res. Lett.*, 44, 10691–10701,
<https://doi.org/10.1002/2017gl074532>, 2017.
- Kurokawa, J. and Ohara, T.: Long-term historical trends in air pollutant emissions in Asia: Regional Emission inventory in
650 ASia (REAS) version 3, *Atmos. Chem. Phys.*, 20, 12761–12793, <https://doi.org/10.5194/acp-20-12761-2020>, 2020.
- Lacis, A., Hansen, J., Lee, P., Mitchell, T., and Lebedeff, S.: Greenhouse effect of trace gases, 1970-1980, *Geophys. Res.
Lett.*, 8, 1035–1038, <https://doi.org/10.1029/GL008i010p01035>, 1981.
- Langford, A. O., Brioude, J., Cooper, O. R., Senff, C. J., Alvarez II, R. J., Hardesty, R. M., Johnson, B. J., and Oltmans, S.
J.: Stratospheric influence on surface ozone in the Los Angeles area during late spring and early summer of 2010, *J.*
655 *Geophys. Res.*, 117, D00V06, <https://doi.org/10.1029/2011JD016766>, 2012.
- Langford, A. O., Alvarez, R. J., Brioude, J., Evan, S., Iraci, L. T., Kirgis, G., Kuang, S., Leblanc, T., Newchurch, M. J.,
Pierce, R. B., Senff, C. J., and Yates, E. L.: Coordinated profiling of stratospheric intrusions and transported pollution by the
Tropospheric Ozone Lidar Network (TOLNet) and NASA Alpha Jet experiment (AJAX): Observations and comparison to
HYSPLIT, RAQMS, and FLEXPART, *Atmos. Environ.*, 174, 1–14, <https://doi.org/10.1016/j.atmosenv.2017.11.031>, 2018.
- 660 Lee, T., Go, S., Lee, Y. G., Park, S. S., Park, J., and Koo, J.-H.: Temporal variability of surface air pollutants in megacities
of South Korea, *Front. Environ. Sci.*, 10, 915531, <https://doi.org/10.3389/fenvs.2022.915531>, 2022.
- Li, S., Yang, Y., Wang, H., Li, P., Li, K., Ren, L., Wang, P., Li, B., Mao, Y., and Liao, H.: Rapid increase in tropospheric
ozone over Southeast Asia attributed to changes in precursor emission source regions and sectors, *Atmos. Environ.*, 305,
119776, <https://doi.org/10.1016/j.atmosenv.2023.119776>, 2023.
- 665 Li, M., Kurokawa, J., Zhang, Q., Woo, J.-H., Morikawa, T., Chatani, S., Lu, Z., Song, Y., Geng, G., Hu, H., Kim, J., Cooper,
O. R., and McDonald, B. C.: MIXv2: a long-term mosaic emission inventory for Asia (2010–2017), *Atmos. Chem. Phys.*,
24, 3925–3952, <https://doi.org/10.5194/acp-24-3925-2024>, 2024.
- Lin, M., Fiore, A. M., Cooper, O. R., Horowitz, L. W., Langford, A. O., Levy II, H., Johnson, B. J., Naik, V., Oltmans, S. J.,
and Senff, C. J.: Springtime high surface ozone events over the western United States: Quantifying the role of stratospheric
670 intrusions, *J. Geophys. Res.*, 117, D00V22, <https://doi.org/10.1029/2012JD018151>, 2012.
- Lin, M., Horowitz, L. W., Oltmans, S. J., Fiore, A. M., and Fan, S.: Tropospheric ozone trends at Mauna Loa Observatory
tied to decadal climate variability, *Nat. Geosci.*, 7, 136–143, <https://doi.org/10.1038/ngeo2066>, 2014.



- Lin, M., Fiore, A. M., Horowitz, L. W., Langford, A. O., Oltmans, S. J., Tarasick, D., and Rieder, H. E.: Climate variability modulates western US ozone air quality in spring via deep stratospheric intrusions, *Nat. Commun.*, 6, 7105, 675 <https://doi.org/10.1038/ncomms8105>, 2015.
- Lin, M., et al.: US surface ozone trends and extremes from 1980 to 2014: quantifying the roles of rising Asian emissions, domestic controls, wildfires, and climate, *Atmos. Chem. Phys.*, 17, 2943–2970, <https://doi.org/10.5194/acp-17-2943-2017>, 2017.
- Liu, J., Strode, S. A., Liang, Q., Oman, L. D., Colarco, P. R., Fleming, E. L., et al.: Change in tropospheric ozone in the 680 recent decades and its contribution to global total ozone, *J. Geophys. Res.-Atmos.*, 127, e2022JD037170, <https://doi.org/10.1029/2022JD037170>, 2022.
- Liu, J., Cohen, J. B., He, Q., et al.: Accounting for NO_x emissions from biomass burning and urbanization doubles existing inventories over South, Southeast and East Asia, *Commun. Earth Environ.*, 5, 255, <https://doi.org/10.1038/s43247-024-01424-5>, 2024.
- 685 Logan, J. A.: An analysis of ozonesonde data for the troposphere: Recommendations for testing 3-D models and development of a gridded climatology for tropospheric ozone, *J. Geophys. Res.*, 104, 16115–16149, 1999.
- Lu, X., Hong, J., Zhang, L., Cooper, O. R., Schultz, M. G., Xu, X., Wang, T., Gao, M., Zhao, Y., and Zhang, Y.: Severe surface ozone pollution in China: a global perspective, *Environ. Sci. Technol. Lett.*, 5, 487–494, <https://doi.org/10.1021/acs.estlett.8b00366>, 2018.
- 690 Lu, X., et al.: Tropospheric ozone trends and attributions over East and Southeast Asia in 1995–2019: An integrated assessment using statistical methods, machine learning models, and multiple chemical transport models, *EGUsphere* [preprint], <https://doi.org/10.5194/egusphere-2024-3702>, 2024.
- Malashock, D. A., DeLang, M. N., Jacob, S. B., Serre, M. L., West, J. J., Chang, K.-L., Cooper, O. R., and Anenberg, S. C.: Estimates of ozone concentrations and attributable mortality in urban, peri-urban and rural areas worldwide in 2019, 695 *Environ. Res. Lett.*, 17, 054023, <https://doi.org/10.1088/1748-9326/ac66f3>, 2022.
- McDuffie, E. E., Smith, S. J., O'Rourke, P., Tibrewal, K., Venkataraman, C., Marais, E. A., Zheng, B., Crippa, M., Brauer, M., and Martin, R. V.: A global anthropogenic emission inventory of atmospheric pollutants from sector- and fuel-specific sources (1970–2017): an application of the Community Emissions Data System (CEDS), *Earth Syst. Sci. Data*, 12, 3413–3442, <https://doi.org/10.5194/essd-12-3413-2020>, 2020.
- 700 McPeters, R., Kroon, M., Labow, G., Brinksma, E., Balis, D., Petropavlovskikh, I., Veefkind, J. P., Bhartia, P. K., and Levelt, P. F.: Validation of the Aura Ozone Monitoring Instrument total column ozone product, *J. Geophys. Res.*, 113, D15S14, <https://doi.org/10.1029/2007JD008802>, 2008.
- Mills, G., Pleijel, H., Malley, C. S., Sinha, B., Cooper, O. R., et al.: Tropospheric Ozone Assessment Report: Present-day tropospheric ozone distribution and trends relevant to vegetation, *Elem. Sci. Anth.*, 6, 47, 705 <https://doi.org/10.1525/elementa.302>, 2018.



- Miyazaki, K., Bowman, K., Sekiya, T., Eskes, H., Boersma, F., Worden, H., Livesey, N., Payne, V. H., Sudo, K., Kanaya, Y., Takigawa, M., and Ogochi, K.: Chemical Reanalysis Products, NASA Atmospheric Science Data Center (ASDC), <https://doi.org/10.25966/9qgv-fe81>, 2019a.
- Miyazaki, K., Sekiya, T., Fu, D., Bowman, K., Kulawik, S., Sudo, K., Walker, T., Kanaya, Y., Takigawa, M., Ogochi, K.,
710 Eskes, H., Boersma, K. F., Thompson, A. M., Gaubert, B., Barre, J., and Emmons, L. K.: Balance of Emission and Dynamical Controls on Ozone During the Korea-United States Air Quality Campaign From Multiconstituent Satellite Data Assimilation, *J. Geophys. Res.-Atmos.*, 124, 387–413, 2019b.
- Miyazaki, K., Bowman, K., Sekiya, T., Eskes, H., Boersma, F., Worden, H., Livesey, N., Payne, V. H., Sudo, K., Kanaya, Y., Takigawa, M., and Ogochi, K.: Updated tropospheric chemistry reanalysis and emission estimates, TCR-2, for 2005–
715 2018, *Earth Syst. Sci. Data*, 12, 2223–2259, <https://doi.org/10.5194/essd-12-2223-2020>, 2020.
- NASA Jet Propulsion Laboratory: Table Mountain atmospheric lidar data [Dataset], Network for the Detection of Atmospheric Composition Change (NDACC), <https://www-air.larc.nasa.gov/missions/ndacc/>, 2022.
- Nisbet, E. G., et al.: Rising atmospheric methane: 2007–2014 growth and isotopic shift, *Global Biogeochem. Cycles*, 30, 1356–1370, <https://doi.org/10.1002/2016GB005406>, 2016.
- 720 Nisbet, E. G., Manning, M. R., Dlugokencky, E. J., Fisher, R. E., Lowry, D., Michel, S. E., et al.: Very strong atmospheric methane growth in the 4 years 2014–2017: Implications for the Paris Agreement, *Global Biogeochem. Cycles*, 33, 318–342, <https://doi.org/10.1029/2018GB006009>, 2019.
- NOAA Global Monitoring Laboratory: Homogenized ozonesonde data archive [Dataset], <https://gml.noaa.gov/ozwv/ozonesonde/>, 2022.
- 725 Oman, L. D., Ziemke, J. R., Douglass, A. R., Waugh, D. W., Lang, C., Rodriguez, J. M., and Nielsen, J. E.: The response of tropical tropospheric ozone to ENSO, *Geophys. Res. Lett.*, 38, L13802, <https://doi.org/10.1029/2011GL047865>, 2011.
- Oman, L. D., Douglass, A. R., Ziemke, J. R., Rodriguez, J. M., Waugh, D. W., and Nielsen, J. E.: The ozone response to ENSO in Aura satellite measurements and a chemistry-climate simulation, *J. Geophys. Res.-Atmos.*, 118, 965–976, <https://doi.org/10.1029/2012JD018546>, 2013.
- 730 Pisso, I., Sollum, E., Grythe, H., Kristiansen, N. I., Cassiani, M., Eckhardt, S., et al.: The Lagrangian particle dispersion model FLEXPART version 10.4, *Geosci. Model Dev.*, 12, 4955–4997, <https://doi.org/10.5194/gmd-12-4955-2019>, 2019.
- Prinn, R. G.: Toward an improved global network for determination of tropospheric ozone climatology and trends, *J. Atmos. Chem.*, 6, 281–298, <https://doi.org/10.1007/BF00053861>, 1988.
- Putero, D., Cristofanelli, P., Chang, K.-L., Dufour, G., Beachley, G., Couret, C., Effertz, P., Jaffe, D. A., Kubistin, D.,
735 Lynch, J., Petropavlovskikh, I., Puchalski, M., Sharac, T., Sive, B. C., Steinbacher, M., Torres, C., and Cooper, O. R.: Fingerprints of the COVID-19 economic downturn and recovery on ozone anomalies at high-elevation sites in North America and western Europe, *Atmos. Chem. Phys.*, 23, 15693–15709, <https://doi.org/10.5194/acp-23-15693-2023>, 2023.
- Ramaswamy, V., et al.: Stratospheric temperature trends: Observations and model simulations, *Rev. Geophys.*, 39, 71–122, 2001.



- 740 Rotman, D. A., et al., Global Modeling Initiative assessment model: Model description, integration, and testing of the transport shell, *J. Geophys. Res.*, 106(D2), 1669–1691, <https://doi.org/10.1029/2000JD900463>, 2001.
- Ryoo, J.-M., et al.: Investigating sources of ozone over California using AJAX airborne measurements and models: assessing the long-range transport, *Atmos. Environ.*, 155, 53–67, <https://doi.org/10.1016/j.atmosenv.2017.02.008>, 2017.
- Saunio, M., Emmons, L., Lamarque, J.-F., Tilmes, S., Wespes, C., Thouret, V., and Schultz, M.: Impact of sampling
745 frequency in the analysis of tropospheric ozone observations, *Atmos. Chem. Phys.*, 12, 6757–6773, <https://doi.org/10.5194/acp-12-6757-2012>, 2012.
- Smith, S. J., Zhou, Y., Kyle, P., Wang, H., and Yu, H.: A Community Emissions Data System (CEDS): Emissions For CMIP6 and Beyond, International Emission Inventory Conference, San Diego, CA, 2015.
- Stauffer, R. M., Thompson, A. M., Kollonige, D. E., Komala, N., Al-Ghazali, H. K., Risdianto, D. Y., Dindang, A., Fairudz
750 bin Jamaluddin, A., Sammathuria, M. K., Zakaria, N. B., Johnson, B. J., and Cullis, P. D.: Dynamical drivers of free-tropospheric ozone increases over equatorial Southeast Asia, *Atmos. Chem. Phys.*, 24, 5221–5234, <https://doi.org/10.5194/acp-24-5221-2024>, 2024.
- Steinbrecht, W., Kubistin, D., Plass-Dülmer, C., Davies, J., Tarasick, D. W., von der Gathen, P., Deckelmann, H., Jepsen, N., Kivi, R., Lyall, N., Palm, M., Notholt, J., Kois, B., Oelsner, P., Allaart, M., Piters, A., Gill, M., Van Malderen, R.,
755 Delcloo, A. W., Sussmann, R., Mahieu, E., Servais, C., Romanens, G., Stübi, R., Ancellet, G., Godin-Beckmann, S., Yamanouchi, S., Strong, K., Johnson, B., Cullis, P., Petropavlovskikh, I., Hannigan, J. W., Hernandez, J.-L., Rodriguez, A. D., Nakano, T., Chouza, F., Leblanc, T., Torres, C., Garcia, O., Röhling, A. N., Schneider, M., Blumenstock, T., Tully, M., Paton-Walsh, C., Jones, N., Querel, R., Strahan, S., Stauffer, R. M., Thompson, A. M., Inness, A., Engelen, R., Chang, K.-L., and Cooper, O. R.: COVID-19 Crisis Reduces Free Tropospheric Ozone Across the Northern Hemisphere, *Geophys. Res. Lett.*, 48, e2020GL091987, <https://doi.org/10.1029/2020GL091987>, 2021.
- 760 Stohl, A., et al.: Stratosphere-troposphere exchange: A review, and what we have learned from STACCATO, *J. Geophys. Res.*, 108, 8516, <https://doi.org/10.1029/2002JD002490>, 2003.
- Strahan, S. E. and Douglass, A. R.: Decline in Antarctic ozone depletion and lower stratospheric chlorine determined from Aura Microwave Limb Sounder observations, *Geophys. Res. Lett.*, 45, 382–390, <https://doi.org/10.1002/2017GL074830>,
765 2018.
- Strode, S. A., Rodriguez, J. M., Logan, J. A., Cooper, O. R., Witte, J. C., Lamsal, L. N., Damon, M., Van Aartsen, B., Steenrod, S. D., and Strahan, S. E.: Trends and variability in surface ozone over the United States, *J. Geophys. Res.-Atmos.*, 120, 9020–9042, <https://doi.org/10.1002/2014JD022784>, 2015.
- Szopa, S., Naik, V., Adhikary, B., Artaxo, P., Berntsen, T., Collins, W. D., et al.: Short-Lived Climate Forcers, in: *Climate Change 2021: The Physical Science Basis. Contribution of Working Group I to the Sixth Assessment Report of the Intergovernmental Panel on Climate Change*, edited by: Masson-Delmotte, V., et al., Cambridge University Press, Cambridge, United Kingdom and New York, NY, USA, 817–922, <https://doi.org/10.1017/9781009157896.008>, 2021.
- 770



- Tarasick, D., Galbally, I. E., Cooper, O. R., Schultz, M. G., Ancellet, G., Leblanc, T., et al.: Tropospheric Ozone Assessment Report: Tropospheric ozone from 1877 to 2016, observed levels, trends and uncertainties, *Elem. Sci. Anth.*, 7, 39, 775 <https://doi.org/10.1525/elementa.376>, 2019.
- Thorp, T., Arnold, S. R., Pope, R. J., Spracklen, D. V., Conibear, L., Knote, C., Arshinov, M., Belan, B., Asmi, E., Laurila, T., Skorokhod, A. I., Nieminen, T., and Petäjä, T.: Late-spring and summertime tropospheric ozone and NO₂ in western Siberia and the Russian Arctic: regional model evaluation and sensitivities, *Atmos. Chem. Phys.*, 21, 4677–4697, <https://doi.org/10.5194/acp-21-4677-2021>, 2021.
- 780 Tong, D., Pan, L., Chen, W., Lamsal, L., Lee, P., Tang, Y., Kim, H., Kondragunta, S., and Stajner, I.: Impact of the 2008 Global Recession on air quality over the United States: Implications for surface ozone levels from changes in NO_x emissions, *Geophys. Res. Lett.*, 43, 9280–9288, <https://doi.org/10.1002/2016GL069885>, 2016.
- U.S. EPA: Integrated Science Assessment for Ozone and Related Photochemical Oxidants, EPA/600/R-20/012, April 2020.
- U.S. EPA: Policy Assessment for the Reconsideration of the Ozone National Ambient Air Quality Standards, External 785 Review Draft Version 2, 2023.
- Van Malderen, R., et al.: Ground-based Tropospheric Ozone Measurements: Regional tropospheric ozone column trends from the TOAR-II/HEGIFTOM homogenized datasets, *EGUsphere [preprint]*, <https://doi.org/10.5194/egusphere-2024-3745>, 2025.
- Verstraeten, W. W., Neu, J. L., Williams, J. E., Bowman, K. W., Worden, J. R., and Boersma, K. F.: Rapid increases in 790 tropospheric ozone production and export from China. *Nat. Geosci.* 8: 690–695, <https://doi.org/10.1038/ngeo2493>, 2015.
- Wang, T., Dai, J., Lam, K. S., Nan Poon, C., and Brasseur, G. P.: Twenty-five years of lower tropospheric ozone observations in tropical East Asia: The influence of emissions and weather patterns, *Geophys. Res. Lett.*, 46, 11463–11470, <https://doi.org/10.1029/2019GL084459>, 2019.
- Wang, H., Lu, X., Jacob, D. J., Cooper, O. R., Chang, K.-L., Li, K., Gao, M., Liu, Y., Sheng, B., Wu, K., Wu, T., Zhang, J., 795 Sauvage, B., Nédélec, P., Blot, R., and Fan, S.: Global tropospheric ozone trends, attributions, and radiative impacts in 1995–2017: an integrated analysis using aircraft (IAGOS) observations, ozonesonde, and multi-decadal chemical model simulations, *Atmos. Chem. Phys.*, 22, 13753–13782, <https://doi.org/10.5194/acp-22-13753-2022>, 2022.
- Wang, X., et al.: Rapidly Changing Emissions Drove Substantial Surface and Tropospheric Ozone Increases Over Southeast Asia, *Geophys. Res. Lett.*, 49, e2022GL100223, <https://doi.org/10.1029/2022GL100223>, 2022.
- 800 Wasserstein, R. L., Schirm, A. L., and Lazar, N. A.: Moving to a world beyond $p < 0.05$, *Am. Stat.*, 73, 1–29, <https://doi.org/10.1080/00031305.2019.1583913>, 2019.
- WHO: WHO global air quality guidelines. Particulate matter (PM_{2.5} and PM₁₀), ozone, nitrogen dioxide, sulfur dioxide and carbon monoxide, World Health Organization, Geneva, 2021.
- WMO: State of the Global Climate 2024, WMO-No. 1368, World Meteorological Organization, 2024.



- 805 Xue, L., Ding, A., Cooper, O., Huang, X., Wang, W., Zhou, D., Wu, Z., McClure-Begley, A., Petropavlovskikh, I., Andreae, M. O., and Fu, C.: ENSO and Southeast Asian biomass burning modulate subtropical trans-Pacific ozone transport, *Natl. Sci. Rev.*, 8, nwaa132, <https://doi.org/10.1093/nsr/nwaa132>, 2021.
- Yates, E. L., Iraci, L. T., Kulawik, S. S., Ryoo, J.-M., Marrero, J. E., Parworth, C. L., St. Clair, J. M., Hanisco, T. F., Bui, T. P. V., Chang, C. S., and Dean-Day, J. M.: An extensive database of airborne trace gas and meteorological observations from
810 the Alpha Jet Atmospheric eXperiment (AJAX), *Earth Syst. Sci. Data*, 15, 2375–2389, <https://doi.org/10.5194/essd-15-2375-2023>, 2023.
- Zhao, Y., Saunio, M., Bousquet, P., Lin, X., Berchet, A., Hegglin, M. I., Canadell, J. G., Jackson, R. B., Deushi, M., Jöckel, P., Kinnison, D., Kirner, O., Strode, S., Tilmes, S., Dlugokencky, E. J., and Zheng, B.: On the role of trend and variability in the hydroxyl radical (OH) in the global methane budget, *Atmos. Chem. Phys.*, 20, 13011–13022,
815 <https://doi.org/10.5194/acp-20-13011-2020>, 2020.
- Zhang, L., Jacob, D. J., Boersma, K. F., Jaffe, D. A., Olson, J. R., Bowman, K. W., Worden, J. R., Thompson, A. M., Avery, M. A., Cohen, R. C., Dibb, J. E., Flock, F. M., Fuelberg, H. E., Huey, L. G., McMillan, W. W., Singh, H. B., and Weinheimer, A. J.: Transpacific transport of ozone pollution and the effect of recent Asian emission increases on air quality in North America: an integrated analysis using satellite, aircraft, ozonesonde, and surface observations, *Atmos. Chem. Phys.*,
820 8, 6117–6136, <https://doi.org/10.5194/acp-8-6117-2008>, 2008.
- Zhang, Y., Cooper, O. R., Gaudel, A., Thompson, A. M., Nédélec, P., Ogino, S.-Y., and West, J. J.: Tropospheric ozone change from 1980 to 2010 dominated by equatorward redistribution of emissions, *Nat. Geosci.*, 9, 875–879, <https://doi.org/10.1038/ngeo2827>, 2016.
- Ziemke, J. R., Chandra, S., Duncan, B. N., Froidevaux, L., Bhartia, P. K., Levelt, P. F., and Waters, J. W.: Tropospheric
825 ozone determined from Aura OMI and MLS: Evaluation of measurements and comparison with the Global Modeling Initiative’s Chemical Transport Model, *J. Geophys. Res.*, 111, D19303, <https://doi.org/10.1029/2006JD007089>, 2006.
- Ziemke, J. R., et al.: Tropospheric ozone variability in the tropics from ENSO to MJO and shorter timescales, *Atmos. Chem. Phys.*, 15, 8037–8049, <https://doi.org/10.5194/acp-15-8037-2015>, 2015.
- Ziemke, J. R., Oman, L. D., Strode, S. A., Douglass, A. R., Olsen, M. A., McPeters, R. D., Bhartia, P. K., Froidevaux, L.,
830 Labow, G. J., Witte, J. C., Thompson, A. M., Haffner, D. P., Kramarova, N. A., Frith, S. M., Huang, L.-K., Jaross, G. R., Sefstor, C. J., Deland, M. T., and Taylor, S. L.: Trends in global tropospheric ozone inferred from a composite record of TOMS/OMI/MLS/OMPS satellite measurements and the MERRA-2 GMI simulation, *Atmos. Chem. Phys.*, 19, 3257–3269, <https://doi.org/10.5194/acp-19-3257-2019>, 2019.